

## Two Photoaffinity Analogues of the Tripeptide, Hemiasterlin, Exclusively Label $\alpha$ -Tubulin

Maria Nunes,<sup>\*,‡</sup> Joshua Kaplan,<sup>§</sup> Joseph Wooters,<sup>||</sup> Malathi Hari,<sup>‡</sup> Albert A. Minnick, Jr.,<sup>⊥</sup> Michael K. May,<sup>⊥</sup> Celine Shi,<sup>‡</sup> Sylvia Musto,<sup>‡</sup> Carl Beyer,<sup>‡</sup> Girija Krishnamurthy,<sup>@</sup> Yongchang Qiu,<sup>||</sup> Frank Loganzo,<sup>‡</sup> Semiramis Ayral-Kaloustian,<sup>§</sup> Arie Zask,<sup>§</sup> and Lee M. Greenberger<sup>‡,⊗</sup>

Oncology Research, Chemical and Screening Sciences, Radiosynthesis Group, and Bioorganic Enzymology, Wyeth Research, 401 North Middletown Road, Pearl River, New York 10965, and Protein Chemistry and Proteomics, Wyeth Pharmaceuticals, 200 Cambridge Park Drive, Cambridge, Massachusetts 02140

Received December 1, 2004; Revised Manuscript Received February 15, 2005

**ABSTRACT:** A synthetic analogue of the tripeptide hemiasterlin, designated HTI-286, depolymerizes microtubules, is a poor substrate for P-glycoprotein, and inhibits the growth of paclitaxel-resistant tumors in xenograft models. Two radiolabeled photoaffinity analogues of HTI-286, designated 4-benzoyl-*N*, $\beta$ , $\beta$ -trimethyl-L-phenylalanyl-*N*<sup>1</sup>-[(1*S*,2*E*)-3-carboxy-1-isopropylbut-2-enyl]-*N*<sup>1</sup>,3-dimethyl-L-valinamide (probe 1) and *N*, $\beta$ , $\beta$ -trimethyl-L-phenylalanyl-4-benzoyl-*N*-[(1*S*,2*E*)-3-carboxy-1-isopropyl-2-butenyl]-*N*, $\beta$ , $\beta$ -trimethyl-L-phenylalaninamide (probe 2), were made to help identify HTI-286 binding sites in tubulin. HTI-286, probe 1, and probe 2 had similar affinities for purified tubulin [apparent  $K_{D(\text{app})}$  = 0.2–1.1  $\mu$ M], inhibited polymerization of purified tubulin  $\sim$ 80%, and were potent inhibitors of cell growth (IC<sub>50</sub> = 1.0–22 nM). Both radiolabeled probes labeled exclusively  $\alpha$ -tubulin. Labeling by [<sup>3</sup>H]probe 1 was inhibited by probe 1, HTI-286, vinblastine, or dolastatin 10 (another peptide antimitotic agent that depolymerizes microtubules) but was either unaffected or enhanced (at certain temperatures) by colchicine or paclitaxel. [<sup>3</sup>H]Probe 1 also labeled exclusively tubulin in cytosolic extracts of whole cells. The major, if not exclusive, contact site for probe 1 was mapped to residues 314–339 of  $\alpha$ -tubulin and corresponds to the sheet 8 and helix 10 region. This region is known to (1) have longitudinal interactions with  $\beta$ -tubulin across the interdimer interface, (2) have lateral interactions with adjacent protofilaments, and (3) contact the N-terminal region of stathmin, a protein that induces depolymerization of tubulin. Binding of probe 1 to this region may alter the conformation of tubulin outside the labeling domain, since enzymatic removal of the C-terminus of only  $\alpha$ -tubulin by subtilisin after, but not before, photolabeling is blocked by probe 1. These results suggest that hemiasterlin is in close contact with  $\alpha$ -tubulin and may span the interdimer interface so that it contacts the vinblastine- and dolastatin 10-binding sites believed to be in  $\beta$ -tubulin. In addition, we speculate that antimitotic peptides mimic the interaction of stathmin with tubulin.

$\alpha$ - and  $\beta$ -tubulin heterodimers can polymerize to form the protofilaments that compose microtubules. Since microtubules are essential for mitosis, motility, and proliferation, this helps to explain why agents that bind tubulin and disrupt its function have utility in the control of cancer (1). There are a variety of structurally and functionally diverse antimicrotubule agents. Their mechanism of action remains incompletely understood (2, 3). While low concentrations of all antimicrotubule agents repress the dynamic instability of microtubules, at high stoichiometric ratios compared with tubulin heterodimers (i.e., 1:1), antimicrotubule agents can be divided into two categories: (1) depolymerizing agents such as colchicine, vinca alkaloids, and peptidelike molecules

(exemplified by dolastatin 10) and (2) polymerizing agents such as taxanes and epothilones. The types of agents can be further subdivided by their distinct binding sites within tubulin. On the basis of crystallographic analyses with tubulin stabilized by zinc or stathmin (a protein that regulates microtubule polymerization), it has been determined that colchicine binds within the intradimer interface (4) while taxanes (5) and epothilones (6) bind within overlapping but distinct regions of  $\beta$ -tubulin. The binding domain of vinca alkaloids and dolastatin 10 has been poorly defined. Since these molecules noncompetitively inhibit the binding of each other to tubulin, the binding sites are distinct but related (7). On the basis of cross-linking studies, a portion of vinblastine and dolastatin 10 are likely to make contact with residues 175–213 and Cys<sup>12</sup> of  $\beta$ -tubulin, respectively (8, 9).

The purpose of this study was to determine the binding site for a class of peptidelike inhibitors of tubulin known as hemiasterlins. Hemiasterlins, originally isolated from marine sponges (10–12), are tripeptides that depolymerize tubulin (13). It is one of a class of peptides and depsipeptides, including dolastatin 10, cryptophycin 1, and phomopsin A,

\* To whom correspondence should be addressed. Telephone: (845) 602-5339. Fax: (845) 602-5557. E-mail: nunesm@wyeth.com.

<sup>‡</sup> Oncology Research, Wyeth Research.

<sup>§</sup> Chemical and Screening Sciences, Wyeth Research.

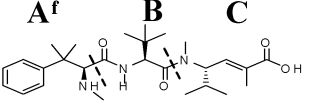
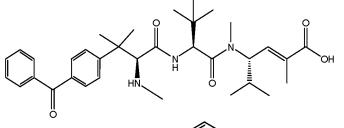
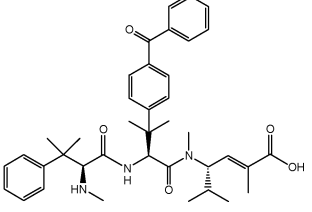
<sup>||</sup> Protein Chemistry and Proteomics, Wyeth Pharmaceuticals.

<sup>⊥</sup> Radiosynthesis Group, Wyeth Research.

<sup>@</sup> Bioorganic Enzymology, Wyeth Research.

<sup>⊗</sup> Current address: Johnson & Johnson, Oncology Research, PROUS, OMP Building, Room B-354, 1000 Route 202, Raritan, NJ 08869.

Table 1: Photoaffinity Probes for HTI-286

Compound	Structure	$K_D^c$ ( $\mu$ M)	$IC_{50}$ KB-3-1 cells <sup>d</sup> (nM)	% inhibition of tubulin polymerization <sup>e</sup>
HTI-286		$0.3 \pm 0.01$	$0.96 \pm 0.5$ (n=79)	$87.5 \pm 12.2$ (n = 48)
Probe 1 <sup>a</sup>		$0.2 \pm 0.01$	$1.8 \pm 0.1$ (n=2)	88
Probe 2 <sup>b</sup>		$1.1 \pm 0.33$	$22.4 \pm 0.7$ (n=2)	69

<sup>a</sup> The chemical name for probe 1 is 4-benzoyl-*N*, $\beta$ , $\beta$ -trimethyl-L-phenylalanyl-*N*<sup>1</sup>-[(1*S*,2*E*)-3-carboxy-1-isopropylbut-2-enyl]-*N*<sup>1</sup>,3-dimethyl-L-valinamide. It has been tritiated within the benzene rings: specific activity of 70.6 Ci/mmol, purity of >99%. <sup>b</sup> The chemical name for probe 2 is *N*, $\beta$ , $\beta$ -trimethyl-L-phenylalanyl-4-benzoyl-*N*-[(1*S*,2*E*)-3-carboxy-1-isopropyl-2-butenyl]-*N*, $\beta$ , $\beta$ -trimethyl-L-phenylalaninamide. It has been tritiated within the benzene rings of the benzophenone group: specific activity of 82.1 Ci/mmol, purity of >98.8%. <sup>c</sup> Affinity constant (mean  $\pm$  standard error) determined by binding of a non-radiolabeled probe to tubulin by fluorescence analysis as described in Materials and Methods. <sup>d</sup> KB cells were grown in the presence of the test agent for 72 h according to the method of Loganzo et al. (21). Cell survival was determined by the sulforhodamine B method.  $IC_{50}$  is the mean concentration of drug needed to inhibit cell growth by 50%  $\pm$  standard error. <sup>e</sup> Bovine brain tubulin was allowed to polymerize in the absence or presence of 0.3  $\mu$ M test agent according to previously described methods (21). The value is the mean  $\pm$  standard error; no standard error is shown for a single determination. <sup>f</sup> The individual amino acids of hemiasterlin are indicated by the A–C subunits.

that are likely to interact with tubulin in a similar manner (7). In support of this, competitive inhibition of binding of dolastatin 10 to tubulin has been observed with hemiasterlin (14) and cryptophycin 1 (15). In contrast, noncompetitive inhibition of binding of vinca alkaloid to tubulin has been observed with cryptophycin 1 (15), hemiasterlin (14), and dolastatin 10 (16). All of these molecules destabilize microtubules by inducing the formation of nonmicrotubule rings, spirals, and oligomers, albeit of different sizes (7). Our interest in hemiasterlin stems from a synthetic analogue of the natural product, HTI-286 (also known as SPA-110) (17, 18), which may have clinical utility since unlike paclitaxel or vinca alkaloids, it has a weak interaction with P-glycoprotein, does not lead to overexpression of P-glycoprotein in cells selected for resistance to HTI-286 (19, 20), and overcomes P-glycoprotein-mediated taxane resistance in vitro and in xenograft models (21). Clinical trials with HTI-286 are in progress (22).

At present, little is known about the site of interaction of peptides with tubulin. Direct photoaffinity labeling studies place a binding site of dolastatin 10 within the amino-terminal peptide of  $\beta$ -tubulin containing cysteine 12 (9). Using molecular modeling methods, two groups have placed the binding site for two peptides (hemiasterlin and cryptophycin 52) near helices 6 and 7 of  $\beta$ -tubulin and helix 10 of  $\alpha$ -tubulin (23, 24). It is reported here that two radiolabeled benzophenone photoaffinity probes of HTI-286 (shown in Table 1) bind exclusively within  $\alpha$ -tubulin. On the basis of peptide mapping studies that have been performed with one of these probes, a major photoaffinity binding site is located within amino acid residues 314–339 that corresponds to the

$\beta$ -sheet 8 and helix 10 region of  $\alpha$ -tubulin. This region is believed to have longitudinal interactions with  $\beta$ -tubulin (across the interdimer interface) and lateral interactions with protofilaments (25). The labeling site is the same site at which the N-terminus of stathmin binds specifically to  $\alpha$ -tubulin (4, 26, 27).

## EXPERIMENTAL PROCEDURES

**Reagents.** HTI-286 {*N*, $\beta$ , $\beta$ -trimethyl-L-phenylalanyl-*N*<sup>1</sup>-[(1*S*,2*E*)-3-carboxy-1-isopropylbut-2-enyl]-*N*<sup>1</sup>,3-dimethyl-L-valinamide trifluoroacetate} was synthesized as previously reported (18). Two benzophenone photoaffinity analogues of HTI-286 were made (Table 1) (28). Probe 1<sup>1</sup> is 4-benzoyl-*N*, $\beta$ , $\beta$ -trimethyl-L-phenylalanyl-*N*<sup>1</sup>-[(1*S*,2*E*)-3-carboxy-1-isopropylbut-2-enyl]-*N*<sup>1</sup>,3-dimethyl-L-valinamide (28). Probe 2 is *N*, $\beta$ , $\beta$ -trimethyl-L-phenylalanyl-4-benzoyl-*N*-[(1*S*,2*E*)-3-carboxy-1-isopropyl-2-butenyl]-*N*, $\beta$ , $\beta$ -trimethyl-L-phenylalaninamide. Bovine brain tubulin (99% pure), HeLa cell tubulin (90% pure), guanosine 5'-triphosphate (GTP), and PEM buffer [80 mM piperazine-*N*,*N'*-bis(2-ethanesulfonic acid) (PIPES) containing 1 mM ethylenebis(oxyethyleneni-

<sup>1</sup> Abbreviations: CNBr, cyanogen bromide; DMSO, dimethyl sulfoxide; DTT, dithiothreitol; IAM, iodoacetamide; MS, mass spectrometry; PEM, 80 mM piperazine-*N*,*N'*-bis(2-ethanesulfonic acid) (PIPES) containing 1 mM ethylenebis(oxyethylenenitrilo)tetraacetic acid (EGTA) and 1 mM MgCl<sub>2</sub>; PMSF, phenylmethanesulfonyl fluoride; probe 1, 4-benzoyl-*N*, $\beta$ , $\beta$ -trimethyl-L-phenylalanyl-*N*<sup>1</sup>-[(1*S*,2*E*)-3-carboxy-1-isopropylbut-2-enyl]-*N*<sup>1</sup>,3-dimethyl-L-valinamide; probe 2, *N*, $\beta$ , $\beta$ -trimethyl-L-phenylalanyl-4-benzoyl-*N*-[(1*S*,2*E*)-3-carboxy-1-isopropyl-2-butenyl]-*N*, $\beta$ , $\beta$ -trimethyl-L-phenylalaninamide; tubulin-S, tubulin digested with subtilisin; RT, room temperature.

trilo)tetraacetic acid (EGTA) and 1 mM magnesium chloride (pH 6.8)] were obtained from Cytoskeleton (Denver, CO). Paclitaxel, vinblastine, colchicine, leupeptin, dimethyl sulfoxide (DMSO), phenylmethanesulfonyl fluoride (PMSF), sodium dodecyl sulfate (SDS), and subtilisin were obtained from Sigma (St. Louis, MO). Dolastatin 10 was kindly provided by the National Cancer Institute (Frederick, MD). Compounds were prepared as 1 or 10 mM stocks in DMSO for competition studies. Trypsin treated with L-(tosylamido-2-phenyl) ethyl chloromethyl ketone (TPCK) was obtained from Worthington Biochemical Corp. (Freehold, NJ) or Promega (Madison, WI). LysC was from Wako Chemicals (Richmond, VA). Formic acid, cyanogen bromide (CNBr), iodoacetamide (IAM), dithiothreitol (DTT), and trifluoroacetic acid (TFA) were obtained from Pierce (Rockford, IL). Guanidine hydrochloride was obtained from Aldrich Chemical Co., Inc. (Milwaukee, WI). Acetic acid, methanol, and acetonitrile were from Fisher Scientific (Fair Lawn, NJ). Beckman tissue solubilizer-450 (BTS-450) and liquid scintillation cocktail (Ready protein) were obtained from Beckman Coulter Instruments, Inc. (Fullerton, CA). EN<sup>3</sup>HANCE autoradiography enhancer was obtained from NEN Life Science Products, Inc. (Boston, MA). Precast gels used for electrophoresis were obtained from Bio-Rad (Hercules, CA).

**Preparation of Radiolabeled Probes 1 and 2.** Tritiated probes 1 and 2 were prepared by direct tritium exchange labeling of the corresponding unlabeled compounds using Crabtree's catalyst, (1,5-cyclooctadiene)(pyridine)(tricyclohexylphosphine)iridium(I) hexafluorophosphate (29, 30). This catalyst is now commonly used for the introduction of tritium labels into aromatic positions, especially those positions ortho to benzophenone carbonyl groups (31–35). A solution of unlabeled probe 1 trifluoroacetic acid (TFA) salt (1 mg, 1.6  $\mu$ mol) and Crabtree's catalyst [5 mg, 6.4  $\mu$ mol, 4.0 equiv; purchased from Aldrich (St. Louis, MO)] in methylene chloride (1.00 mL) was exposed to 3.90 Ci of pure tritium gas (0.20 atm) overnight followed by workup, removal of all volatile tritium, and HPLC purification on a Phenomenex Prodigy 5  $\mu$ m ODS(3) semipreparative HPLC column [250 mm (length)  $\times$  10 mm (inside diameter)] with an aqueous acetonitrile (0.02% TFA) gradient. A total of 89.9 mCi of tritiated [<sup>3</sup>H]probe 1 was recovered with a radiochemical purity of >98%. The specific activity was determined to be 70.6 Ci/mmol by LC–MS, with an average of 2.45 tritium atoms per molecule. Proton (600 MHz) and tritium (640 MHz) NMR (in *d*<sub>6</sub>-DMSO solvent) established that the labels were in aromatic positions as expected. Similarly, a solution of unlabeled photolabel 2 bis-TFA salt (1.4 mg, 1.6  $\mu$ mol) and Crabtree's catalyst (6.5 mg, 8.0  $\mu$ mol, 5.0 equiv) in methylene chloride (1.00 mL) was exposed to 3.79 Ci of pure tritium gas (0.21 atm) overnight followed by workup, removal of all volatile tritium, and HPLC purification as described above. A total of 93.5 mCi of tritiated [<sup>3</sup>H]probe 2 was recovered with a radiochemical purity of >98%. The specific activity of tritiated photolabel 2 was 82.1 Ci/mmol as determined from LC–MS, with an average of 2.80 tritium atoms per molecule. Similar proton and tritium NMR analysis (also in *d*<sub>6</sub>-DMSO solvent) confirmed the presence of the tritium atoms in aromatic positions.

**Reversible Binding Assay.** The affinity of HTI-286, as well as non-radiolabeled probe 1 and probe 2, for bovine brain

tubulin was determined by previously published methods (36). Briefly, 5 mg/mL rhodamine-labeled tubulin prepared in PEM buffer was preincubated with buffer or varying concentrations of test agents in individual quartz cuvettes. The fluorescence intensity of tubulin (excitation at 560 nm and maximal emission at 580 nm) was measured after preincubation for 90 min. The change in fluorescence intensity at 580 nm was used to estimate the apparent dissociation constant of the test agents using a quadratic equation. The results of this method were confirmed using a second assay. In this case, the binding of radiolabeled probe 1 to bovine brain tubulin was assessed by incubating 0.5  $\mu$ M tubulin with 0.005–5  $\mu$ M probe 1 in the presence or absence of 5  $\mu$ M probe 1 for 30 min at RT in PEM buffer. Binding was assessed using centrifugal gel filtration on Sephadex G-50 (Microspin G-50) as described previously (15). Spin columns (Amersham Biosciences, Piscataway, NJ) were centrifuged for 1 min at 2000 rpm in a microcentrifuge immediately prior to use, and samples were applied in a total volume of 50  $\mu$ L, followed by a 2 min centrifugation at the same speed. The amount of probe 1 bound to tubulin was quantitated by measuring the radioactivity within aliquots collected after centrifugation. The  $K_{D(\text{app})}$  value, representing 50% of specific binding, was calculated from the curve generated by subtracting the amount of radiolabeled probe bound in the absence of probe from that bound in the presence of non-radiolabeled probe.

**Tubulin Polymerization Assays.** For in vitro polymerization assays, bovine MAP-rich tubulin in cold buffer containing PIPES buffer (pH 6.9), 1 mM MgCl<sub>2</sub>, and 1 mM EGTA with 1 mM GTP was first centrifuged at 12000g for 10 min at 4 °C. The tubulin solution (100  $\mu$ L/well) was added to a 96-well dish which already contained 10  $\mu$ L of the test compound in the same solution. The turbidity produced by the reaction was measured at 340 nm every minute for 60 min while the reaction mixture was incubated at 24 °C using a SpectraMAX Plus reader (Molecular Devices, Sunnyvale, CA).

**Photolabeling, SDS–PAGE, and Fluorography.** For labeling with purified tubulin, 2.5  $\mu$ M tubulin (5  $\mu$ g) prepared in PEM buffer was incubated with or without a competitor molecule for 15 min at RT or 4 °C, prior to the addition of the radiolabeled probe (2.5 or 0.25  $\mu$ M) at RT or 37 °C. After 30 min, samples were irradiated at 360 nm with a Mineralight lamp (UVP, Upland, CA) at 4 °C for up to 2 h. Photolabeled samples were analyzed by SDS–PAGE using 7.5% Tris–HCl gels. Low-grade SDS (Sigma, catalog no. L5750) was used in the running buffer, when needed, to allow separation of  $\alpha$ - and  $\beta$ -tubulin subunits. Gels were fixed, stained with Coomassie Blue (Bio-Rad) to ensure equal loading of protein, and then sliced. The radioactivity of each 1 mm slice was determined by placing it overnight at RT in 200  $\mu$ L of 90% BTS-450, followed by addition of 6 mL of Ecolume scintillation cocktail before the vials were subjected to scintillation counting. Alternatively, gels were incubated with EN<sup>3</sup>HANCE according to the manufacturer's instructions (Life Sciences Products, Inc.), washed, and dried prior to exposure of the gel to Biomax MS film (Kodak) for fluorography.

**Photoaffinity Labeling of Cytosolic Preparations of Whole Cell Lysates.** Cell lysates from KB-3-1 epidermoid carcinoma cells were prepared by first rinsing cells in phosphate-



buffered saline followed by scraping the cells into PEM buffer at 4 °C. The cells were then lysed with 30 strokes on ice in a Dounce homogenizer. Nuclei and unbroken cells were removed by centrifugation at 1000g for 10 min. Postnuclear lysate was centrifuged at 100000g for 1 h to separate membranes from the cytosol. The amount of protein in the cytosol was estimated by the Bio-Rad D<sub>C</sub> protein assay. To label this material, 50  $\mu$ g of cytosolic protein was incubated with 2.5  $\mu$ M [<sup>3</sup>H]probe 1 with or without 250  $\mu$ M HTI-286 (final volume of 20  $\mu$ L). After a 30 min incubation at RT in the dark, the sample was irradiated as described above. At the end of the photoactivation, 7  $\mu$ L of 4 $\times$  Laemmli sample buffer was added to the reaction mixtures and the proteins were separated on a 7.5% SDS–PAGE gel. The gel was subjected to fluorography.

**Subtilisin Digestion.** Tubulin (2.5  $\mu$ M) was digested under native conditions with subtilisin (0.2  $\mu$ g; final concentration of 0.37  $\mu$ M) for 15–60 min at 30 °C before or after labeling with 0.25  $\mu$ M (0.36  $\mu$ Ci) probe 1 for 30 min at RT, followed by irradiation as described above. Enzymatic digestion was stopped by adding PMSF to a final concentration of 1 mM. Samples were then resolved by SDS–PAGE under conditions that allowed separation of  $\alpha$ - and  $\beta$ -tubulin subunits. Gels were then fixed and stained with Coomassie Blue (Bio-Rad) and subjected to fluorography.

**Formic Acid Digestion.** For peptide mapping studies, 50  $\mu$ M tubulin, which was photolabeled with 5  $\mu$ M (7.2  $\mu$ Ci) probe 1, was run under gel conditions that allow the  $\alpha$ - and  $\beta$ -tubulin to comigrate. Tubulin was excised from the gel by cutting the unstained gel in the region that comigrated precisely with the 50 kDa marker of the Precision Protein Standards (Bio-Rad). The material was digested in-gel in 250  $\mu$ L of 75% formic acid at 37 °C. After 44–72 h, formic acid was removed in a speed vacuum, and digestion products were separated by SDS–PAGE on Tris-Tricine gels (10–20%). Radiolabeled peptides were visualized by fluorography. In other types of experiments, tubulin subunits were separated on 7.5% Tris-HCl gels (Bio-Rad) and  $\alpha$ - and  $\beta$ -tubulin bands were cut and digested separately. The sequence of the labeled formic acid digestion fragment was confirmed by MS analysis.

**CNBr Digestion.** Tubulin (2.5  $\mu$ M) was photolabeled with 0.25  $\mu$ M probe 1 and  $\alpha$ - and  $\beta$ -tubulin resolved on a 7.5% Tris-Glycine SDS gel. Gel bands were independently excised, reduced with DTT (10 mM in 100 mM ammonium bicarbonate), and alkylated with IAM (25 mM in 100 mM ammonium bicarbonate). The gel bands containing tubulin were shrunk with 100% acetonitrile and reswelled with CNBr (150 mg/mL) in 70% formic acid. Digestion was allowed to proceed for 4.5 h at RT. Gel bands were then evaporated to dryness from H<sub>2</sub>O several times in a vacuum to remove excess reagents. The gel bands were then reswollen with SDS loading buffer and mounted on top of a 10 to 20% Tris-Tricine gel, and the digestion products were separated on a second gel. Replicate gels were run of the CNBr fragments: one gel electroblotted to polyvinylidene difluoride for autoradiography and the other silver stained (37). Blots for autoradiography were first soaked with a solution of PPO in toluene, and autoradiographic images were captured on Kodak BioMax MS film. The 7 kDa CNBr gel fragment was further digested with trypsin as described below. As in the formic acid digestion protocol, the sequence of the labeled

CNBr digestion fragment was confirmed by MS analysis from the silver-stained gel.

**Trypsin Digestion of Native Tubulin.** Native tubulin (7.5  $\mu$ M) was photolabeled with 0.25  $\mu$ M (0.35  $\mu$ Ci) probe 1 and resolved by SDS–PAGE, in PEM buffer at RT. After 30 min, samples were irradiated on ice and then digested with 0.8  $\mu$ g of trypsin for 5–30 min at 30 °C. The reaction was stopped by adding leupeptin to a final concentration of 0.01 mM. The samples were separated on 10 to 20% Tris-Tricine gels. The radioactivity within 1 mm gel slices was determined. Alternatively, peptides were resolved on 7.5% Tris-HCl gels, and gels were then exposed to film using fluorographic methods described above.

**Trypsin and LysC Digestion of Gel-Purified Tubulin.** Tubulin (2.5  $\mu$ M) was photolabeled with 0.25  $\mu$ M probe 1 and  $\alpha$ - and  $\beta$ -isomers resolved in gels. Gel bands were then excised manually after silver staining and digested with sequencing-grade trypsin or LysC using a digestion robot (DigestPro; Abimed, Langenfeld, Germany). The automated protocol was as follows. Gel bands were reduced with DTT (10 mM in 100 mM ammonium bicarbonate) and alkylated with IAM (25 mM in 100 mM ammonium bicarbonate) to stabilize cysteine-containing peptides. Proteins were then digested in the gel overnight at 37 °C (12.5 ng/ $\mu$ L enzyme in 100 mM ammonium bicarbonate and 20% acetonitrile), eluted, concentrated, and subjected to MS analysis.

**MS Analyses.** Peptides from the in-gel enzymatic digestion were injected onto a self-packed PicoFrit C18 column (New Objectives, Woburn, MA) that is directly interfaced with an ion trap mass spectrometer (LCQ Deca, ThermoFinnigan, San Jose, CA). During a 90 min HPLC gradient [from 4 to 60% solvent B (0.1 M acetic acid, 90% ACN, and H<sub>2</sub>O); solvent A, 0.1 M acetic acid and H<sub>2</sub>O], the mass spectrometer was operated in a data-dependent mode using software provided by the manufacturer to acquire both MS (peptide mass) and MS/MS (fragment ion mass) spectra. Peptide sequences were determined by matching the fragment ion spectra against the nonredundant NCBI protein database using the Sequest search algorithm provided by ThermoFinnigan.

**Modeling Methods.** Molecular modeling studies were performed using the Weblab Viewer Lite software (Accelrys, Inc., San Diego, CA). The structure of tubulin was taken from Lowe et al. (5).

## RESULTS

**Photoprobes 1 and 2 Interact with Tubulin in a Manner Similar to That of HTI-286.** Total synthesis of hemiasterlin (38) allowed investigation of the structure–activity relationship (SAR) (17, 18) of this molecule, leading to one well-characterized analogue, HTI-286, with optimal anticancer activity in animal models (21). Further analogue studies on HTI-286 (18) revealed aspects of the SAR of the tripeptide that were crucial to the design of photoprobes 1 and 2. Probes 1 and 2 contain benzophenone moieties in the so-called A and B regions of HTI-286, respectively (Table 1). To compare the affinity of non-radiolabeled probes 1 and 2 with that of HTI-286, compounds were incubated with rhodamine-labeled tubulin derived from bovine brain for 90 min. Under these conditions, the binding of the compound altered the fluorescence intensity derived from tubulin. The apparent

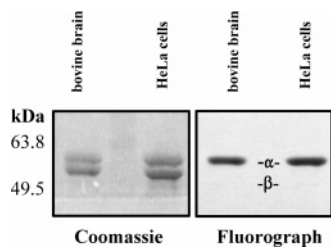


FIGURE 1: Probe 1 photolabels  $\alpha$ -tubulin. Purified bovine brain tubulin ( $2.5 \mu\text{M}$ ) and purified HeLa cell tubulin ( $10 \mu\text{M}$ ) were incubated for 30 min at RT with  $2.5 \mu\text{M}$  ( $3.6 \mu\text{Ci}$ ) [ $^3\text{H}$ ]probe 1. Afterward, samples were irradiated with 360 nm light for 2 h at  $4^\circ\text{C}$ . Protein was resolved in gels under conditions that allowed for the resolution of  $\alpha$ - and  $\beta$ -tubulin. Gels were analyzed by Coomassie Blue staining or fluorography.

$K_D$  values for probes 1 and 2 were determined to be 0.2 and  $1.1 \mu\text{M}$ , respectively; these values were approximately 0.8- and 6-fold higher, respectively, than that obtained for HTI-286 (Table 1). These values were confirmed using an alternative method for binding analysis, where the binding constant was determined by examining the ability of radiolabeled probe 1 to bind to tubulin (in the presence or absence of non-radiolabeled competitor). Under these conditions, an apparent  $K_D$  value of  $0.35 \mu\text{M}$  was calculated and is in close agreement with the fluorescence method. Consistent with these results, the compounds were good inhibitors of microtubule-mediated phenomena. In particular,  $0.3 \mu\text{M}$  HTI-286, probe 1, and probe 2 inhibited tubulin polymerization in a cell-free system by 88, 88, and 69%, respectively (Table 1), using approximately  $10 \mu\text{M}$  tubulin monomer. The fact that HTI-286 analogues inhibit tubulin polymerization at substoichiometric amounts compared with tubulin is not surprising as HTI-286 has a high affinity for tubulin (36). In addition, probes 1 and 2 were potent inhibitors of the proliferation of KB-3-1 cells in tissue culture ( $\text{IC}_{50} = 1.8$  and  $22 \text{ nM}$ , respectively) and therefore have good to moderate potency compared with HTI-286 ( $\text{IC}_{50} = 0.96 \text{ nM}$ ). These data suggest that probe 1, and less so probe 2, are potent inhibitors of tubulin function compared with HTI-286 and other antimicrotubule agents (39).

**Probe 1 Photolabels the  $\alpha$ -Tubulin Subunit.** The binding of the HTI-286 photoaffinity analogue to purified tubulin was evaluated by incubating tubulin derived from bovine brain ( $2.5 \mu\text{M}$ ) or human HeLa cells ( $10 \mu\text{M}$ ) with  $2.5 \mu\text{M}$  [ $^3\text{H}$ ]probe 1 for 30 min at RT followed by irradiation at 360 nm for 2 h at  $4^\circ\text{C}$ . Gel conditions that allow the resolution of  $\alpha$ - and  $\beta$ -tubulin were used. (Two hours of irradiation was chosen since initial experiments indicated that photo-incorporation reached maximum levels at this time.) This photoprobe cross-linked with a species that comigrated with  $\alpha$ -tubulin derived from both sources (Figure 1). Probe 1 appeared to bind exclusively to  $\alpha$ -tubulin even if the irradiation was varied between 5 min and 4 h (data not shown). There was little, if any, evidence that the probe bound to  $\beta$ -tubulin; any labeling that was observed to comigrate with  $\beta$ -tubulin was detected only after the species labeling  $\alpha$ -tubulin was grossly overexposed and could not be definitively distinguished from  $\alpha$ -tubulin. The identification of the higher of the two Coomassie-stained molecular weight species was confirmed to be  $\alpha$ -tubulin using monoclonal antibodies specific for  $\alpha$ - and  $\beta$ -tubulin as well as by MS analysis of the  $\alpha$ - and  $\beta$ -tubulin bands (data not shown).

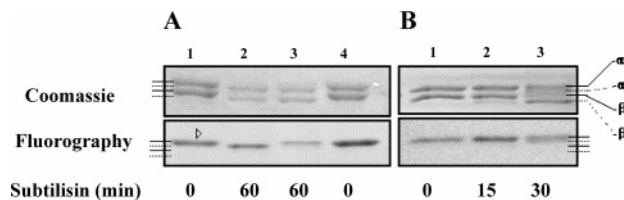
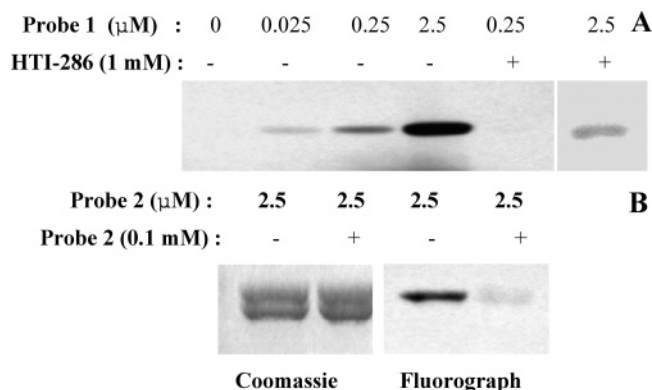


FIGURE 2: Digestion of photolabeled tubulin with subtilisin. (A) Tubulin ( $2.5 \mu\text{M}$ ) was incubated in the absence (lanes 1 and 4) or presence (lane 2) of  $0.2 \mu\text{g}$  of subtilisin for 60 min at  $30^\circ\text{C}$ . The reaction was terminated by the addition of PMSF to a final concentration of  $1 \text{ mM}$  and then photolabeled with  $0.25 \mu\text{M}$  [ $^3\text{H}$ ]probe 1 according to conditions specified in the legend of Figure 1. Alternatively, photolabeling was done before subtilisin digestion (lane 3). In both cases, samples were then separated by SDS-PAGE and stained with Coomassie Blue (top) and radioactive fragments were detected by fluorography (bottom). (B) Tubulin ( $2.5 \mu\text{M}$ ) was incubated in the absence (lane 1) or presence of  $0.05 \mu\text{g}$  of subtilisin (lanes 2 and 3) for 0–30 min at RT, followed by addition of PMSF to a final concentration of  $10 \text{ mM}$ , and labeled with [ $^3\text{H}$ ]probe 1 as described. Samples were resolved on gels as stated above. The positions of  $\alpha$ -tubulin,  $\alpha$ -tubulin-S,  $\beta$ -tubulin, and  $\beta$ -tubulin-S are shown.

Although photolabeled tubulin comigrated in the position of  $\alpha$ -tubulin, it was possible that it actually labeled  $\beta$ -tubulin and the labeled species migrated coincidentally in the position of  $\alpha$ -tubulin. To help rule out this possibility, enzymatic digestion of tubulin by subtilisin was carried out. Subtilisin cleaves the C-terminus of  $\alpha$ -tubulin between Asp<sup>438</sup> and Ser<sup>439</sup> and  $\beta$ -tubulin between Gln-433 and Gly-434 (40). The cleaved protein is termed tubulin-S (41). In the first set of experiments, it was found that treatment of tubulin with  $0.2 \mu\text{g}$  of subtilisin for 60 min caused complete digestion since the molecular mass of  $\alpha$ - and  $\beta$ -tubulin decreased approximately 2 kDa as detected by Coomassie Blue staining of the material resolved in gels (Figure 2A, compare lanes 1 and 2, top panel). If enzyme digestion was done before labeling, a radiolabeled band that comigrated with the position of  $\alpha$ -tubulin-S was detected (Figure 2A, lane 2, bottom panel). When a time course of digestion was repeated with 4-fold less enzyme, it was found that  $\beta$ -tubulin was digested before  $\alpha$ -tubulin (Figure 2B, lanes 2 and 3) and, as reported previously (42), is diagnostic for  $\beta$ -tubulin. After digestion for 15 and 30 min,  $\beta$ -tubulin was partially and almost completely digested, respectively (Figure 2B, lanes 2 and 3, top panel), while  $\alpha$ -tubulin was not and partially digested, respectively. Since the photoaffinity-labeled species comigrated with  $\alpha$ -tubulin after 15 or 30 min (Figure 2B, lanes 2 and 3, bottom panel), it was concluded that probe 1 must label  $\alpha$ -tubulin.

In these sets of experiments, labeling of tubulin with probe 1 prior to digestion with subtilisin was also examined. Surprisingly, the labeled species was not digested at all, while Coomassie-stained tubulin was nearly completely digested (Figure 2A, lane 3). We subsequently found that high concentrations of probe 1 or HTI-286 completely inhibited subtilisin digestion of only  $\alpha$ -tubulin while digestion of  $\beta$ -tubulin was unaffected (data not shown). These data are consistent with previous findings, since vinblastine has been shown to inhibit the digestion of  $\alpha$ -tubulin but not  $\beta$ -tubulin by subtilisin, and this effect may be mediated by alteration of the state of tubulin rather than blockade of the cleavage site by vinblastine (43).



**FIGURE 3:** Probe 1 binding to tubulin is competed with HTI-286, and probe 2 binds to  $\alpha$ -tubulin. (A) Bovine brain tubulin (2.5  $\mu$ M) was incubated without or with 1 mM HTI-286 for 15 min at 4  $^{\circ}$ C, followed by addition of increasing concentrations of [ $^3$ H]probe 1 (from 0.025 to 2.5  $\mu$ M) (from 0.036 to 3.6  $\mu$ Ci). After incubation for 30 min at 37  $^{\circ}$ C, samples were irradiated for 30 min and separated by SDS-PAGE, and gels were exposed to film by fluorography. (B) Like panel A, except 2.5  $\mu$ M [ $^3$ H]probe 2 was used and competed with 0.1 mM probe 2: (left) Coomassie Blue-stained gel and (right) fluorography of the gel.

#### HTI-286 Inhibits Binding of Probes 1 and 2 to Tubulin.

The specificity of photolabeling by probe 1 was demonstrated by preincubating tubulin with 1 mM HTI-286 for 15 min at 4  $^{\circ}$ C, followed by addition of increasing concentrations of radiolabeled probe 1 (0.025–2.5  $\mu$ M) (Figure 3A). Under these conditions, HTI-286 caused complete and >50% inhibition of incorporation of 0.25 or 2.5  $\mu$ M radiolabeled probe 1 into  $\alpha$ -tubulin, respectively. Note that  $\alpha$ -tubulin was the only species labeled and no detection of  $\beta$ -tubulin labeling was found under any condition. When a tubulin: radiolabeled probe 1 ratio of 2.5:0.25 (10:1) was used, tubulin labeling was inhibited 93% by HTI-286. When the ratio was changed to 2.5:2.5 (1:1), conditions used mostly for peptide mapping studies, tubulin labeling was inhibited 82%. The photolabeling specificity for probe 1 was also confirmed by labeling tubulin in the presence of increasing concentrations of radiolabeled probe 1 in the presence or absence of 100  $\mu$ M non-radiolabeled probe 1 (data not shown). Radiolabeled probe 2 also was found to specifically label  $\alpha$ -tubulin (Figure 3B). The labeling was specific since labeling by radiolabeled probe 2 was completely inhibited by 100  $\mu$ M probe 2 (Figure 3B) and 100  $\mu$ M HTI-286 (data not shown).

**Probe 1 Photolabels Only Tubulin within Cytosolic Extracts of Cells.** When 2.5  $\mu$ M [ $^3$ H]probe 1 was irradiated in the presence of a cytosolic fraction from KB-3-1 cells, one species was detected that comigrated at the same position as purified tubulin (Figure 4). This was remarkable, since it was the only labeled species in the presence of many Coomassie Blue-stained proteins. Labeling was specific, since it was competed by 250  $\mu$ M HTI-286. The species labeled in the cytosol is most likely to be  $\alpha$ -tubulin since  $\alpha$ - and  $\beta$ -tubulin derived from the cytosolic preparation were separated in this gel system as determined by immunoblot analysis using  $\alpha$ - and  $\beta$ -tubulin specific antibodies (data not shown), and the radiolabeled band from the extract comigrated very close to, if not in the same place as,  $\alpha$ -tubulin from bovine brain. Furthermore, labeling of a species that comigrated with  $\alpha$ -tubulin was clearly seen when a cytosolic fraction from human ovarian carcinoma 2008 cells was used (data not shown).

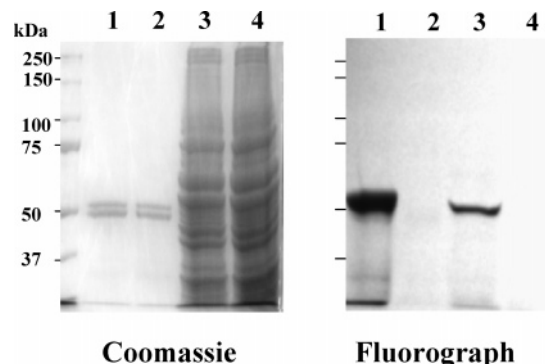


**FIGURE 4:** Labeling of the cytosolic fraction from KB-3-1 cells with probe 1. Bovine brain (BB) tubulin (2.5  $\mu$ M) (lanes 1 and 2) or KB-3-1 cytosol (50  $\mu$ g) (lanes 3 and 4) was incubated with 2.5  $\mu$ M [ $^3$ H]probe 1 in the absence of any competing probe (lanes 1 and 3) or in the presence of 250  $\mu$ M HTI-286 (lanes 2 and 4). After incubation, the samples were irradiated for 2 h at 4  $^{\circ}$ C. Proteins were then resolved by SDS-PAGE and analyzed by Coomassie Blue staining (left) or fluorography (right) of the gel as described in Materials and Methods.

**Table 2:** Competition of the Binding of Probe 1 to Tubulin at RT vs 37  $^{\circ}$ C<sup>a</sup>

competitor (100 $\mu$ M, 400 times)	% control $\pm$ standard error	
	RT	37 $^{\circ}$ C
control	100	100
probe 1	12 $\pm$ 8	24 <sup>b</sup>
dolastatin 10	13 $\pm$ 3	26 <sup>b</sup>
HTI-286	27 $\pm$ 4	47 <sup>b</sup>
vinblastine	28 $\pm$ 1	52 $\pm$ 1
paclitaxel	83 $\pm$ 41	173 $\pm$ 7
colchicine	118 $\pm$ 17	219 $\pm$ 14

<sup>a</sup> Tubulin (2.5  $\mu$ M) was preincubated with the competitor for 15 min at RT, prior to incubation with 0.25  $\mu$ M [ $^3$ H]probe 1 in a 20  $\mu$ L reaction mixture at RT or 37  $^{\circ}$ C for 30 min and irradiated for 2 h at 4  $^{\circ}$ C. Samples were separated as described in Materials and Methods. Results were from two to five independent experiments. <sup>b</sup> Results were from a single experiment.

**Effect of Antimicrotubule Agents and GTP on Competition of Labeling of Tubulin by Probe 1.** Photolabeling was done in the presence or absence of prior incubation with various antimicrotubule agents (Table 2). Initial incubations were done at RT using 2.5  $\mu$ M tubulin and 0.25  $\mu$ M radiolabeled probe 1. Under these conditions, a 400-fold molar excess (100  $\mu$ M) of non-radiolabeled probe 1 and dolastatin 10 reduced the level of labeling by  $\sim$ 87% whereas HTI-286 and vinblastine reduced the level of labeling by  $\sim$ 72%. In contrast, preincubation with paclitaxel and colchicine had almost no effect (Table 2). Since the polymerization state of tubulin can be altered by temperature (44) and may, therefore, alter the binding of HTI-286 to tubulin, experiments in which preincubation was carried out at 37  $^{\circ}$ C were repeated. Under these conditions, non-radiolabeled probe 1 and dolastatin 10 were still the best inhibitors and inhibited labeling by  $\sim$ 75% (Table 2). HTI-286 and vinblastine inhibited labeling by  $\sim$ 50%. However, paclitaxel and colchicine enhanced labeling by 73 and 119%, respectively. The effect of colchicine on probe 1 binding to tubulin was further investigated by preincubating tubulin with 0-, 200-, 400-, 1000-, and 4000-fold molar excesses of colchicine prior to labeling tubulin with probe 1 at 37  $^{\circ}$ C. Under these conditions, colchicine maximally enhanced binding of the probe when used at a 400-fold molar excess (100  $\mu$ M), had



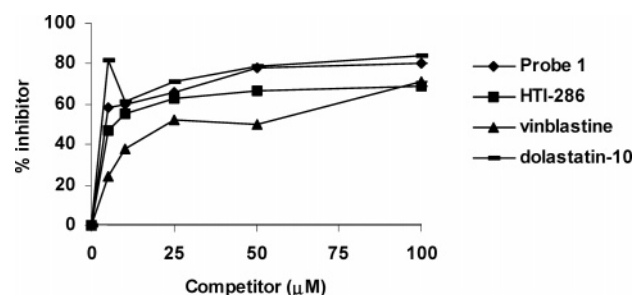


FIGURE 5: Photolabeling of tubulin by probe 1 is strongly inhibited by non-radiolabeled probe 1, dolastatin 10, HTI-286, and vinblastine. Bovine brain tubulin (2.5  $\mu$ M) was preincubated with various concentrations (5–250  $\mu$ M) of non-radiolabeled probe 1, HTI-286, vinblastine, or dolastatin 10 for 15 min at RT, prior to incubation with 0.25  $\mu$ M (0.36  $\mu$ Ci) [ $^3$ H]probe 1 at RT for 30 min. Samples were irradiated for 2 h at 4  $^{\circ}$ C. All samples were separated by SDS–PAGE, and the gels were sliced as described in Materials and Methods to quantitate the amount of radiolabel within tubulin. The concentration of competitor that inhibits tubulin labeling by 50% was obtained from the curves.

less enhancing effects at a 1000-fold molar excess (250  $\mu$ M), and had no effect when used at a 4000-fold excess (1 mM) (data not shown).

The potency of the inhibitory effect of dolastatin 10, HTI-286, and vinblastine on photolabeling was further investigated by determining  $IC_{50}$  values for candidate inhibitors (Figure 5). The same reaction conditions, using incubation at RT, were used as described in Table 2. Under these conditions, probe 1 and dolastatin 10 were equally potent inhibitors of tubulin photolabeling ( $IC_{50} = 5 \mu$ M). HTI-286 was slightly less potent ( $IC_{50} = 7 \mu$ M), while vinblastine was least inhibitory ( $IC_{50} = 22 \mu$ M).

It has been reported that hemiasterlin and dolastatin 10 inhibit GTP exchange in tubulin but do not inhibit the ability of GTP to bind tubulin (14, 16). To further determine if GTP

inhibited the binding of probe 1 to tubulin, tubulin was preincubated with a range of GTP concentrations (0–100  $\mu$ M) prior to photolabeling. Under these conditions, GTP did not significantly inhibit photoincorporation (data not shown).

#### Location of the Probe 1 Photolabeling Site within Tubulin.

The cross-linking efficiency for probe 1 was approximately 1.5% under optimal conditions and found to be sufficient for peptide mapping studies. To map the binding site(s) of probe 1 in purified tubulin, a series of experiments were carried out using chemical and enzymatic digestion of denatured and native tubulin.

Initially, photolabeled tubulin was resolved on 7.5% Tris–HCl SDS–PAGE and the tubulin band (containing  $\alpha$ - and  $\beta$ -subunits that were not resolved from each other) or individual  $\alpha$ - and  $\beta$ -tubulin subunit bands were excised from the gel and digested with formic acid. Formic acid is known to preferentially cleave Asp–Pro bonds (45). Although the sequence of bovine  $\alpha$ -tubulin has not been described,  $\alpha$ -tubulin is extraordinarily conserved across vertebrate species, including those derived from porcine, rat, murine, and human origin, and contains only one such linkage between Asp<sup>306</sup> and Pro<sup>307</sup> (Figure 6A) (46). Therefore, complete formic acid digestion of  $\alpha$ -tubulin derived from bovine tubulin would be expected to produce two distinct peptide fragments consisting of amino acids 1–306 (~34.5 kDa) and 307–451 (~16 kDa) that have been previously identified by immunological methods as the N- and C-terminal portions of tubulin, respectively (47). In contrast, formic acid digestion of  $\beta$ -tubulin is known to produce three fragments consisting of amino acids 1–31 (~3.5 kDa), 32–304 (~31 kDa), and 305–445 (~16 kDa) (48). Upon formic acid in-gel digestion of photolabeled tubulin, three main protein bands were observed (Figure 6B): the upper ~34.5

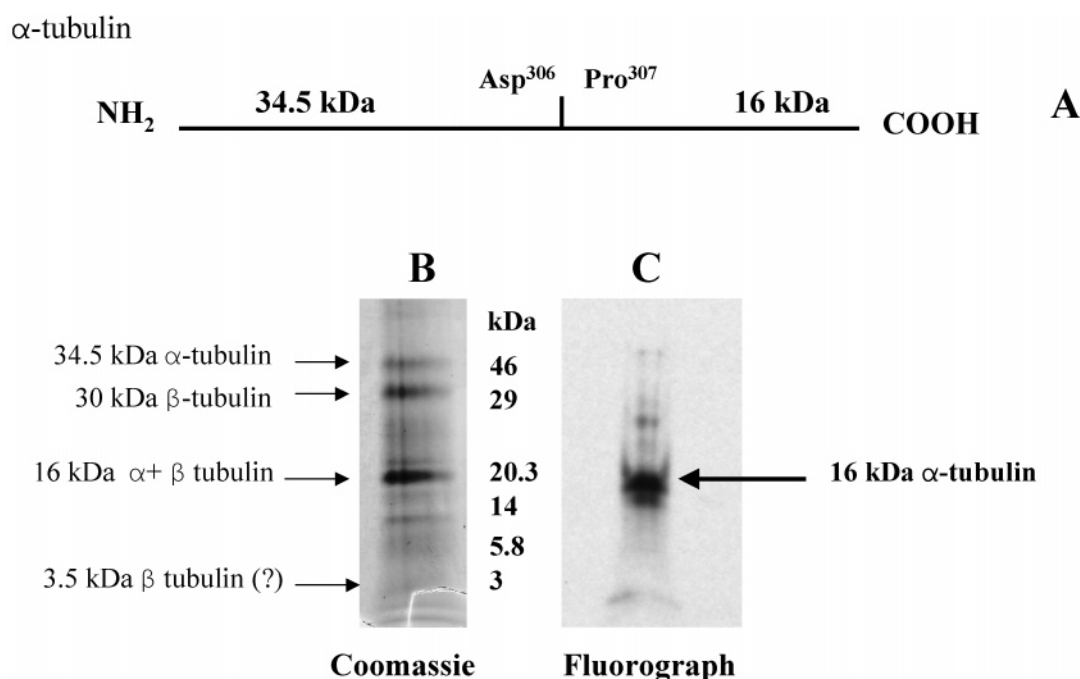


FIGURE 6: Formic acid digestion of probe 1-photolabeled tubulin creates a 16 kDa labeled peptide fragment. Photolabeled tubulin was resolved by SDS–PAGE under conditions that allowed  $\alpha$ - and  $\beta$ -tubulin to comigrate. The tubulin band was excised from gel and digested with 75% formic acid at 37  $^{\circ}$ C. After 72 h, formic acid digestion products were separated on a 10–20% Tris–Tricine gel. A diagram of the predicted formic acid cleavage sites and cleavage products is shown for  $\alpha$ -tubulin (A). The fragments were visualized by Coomassie Blue staining (B) and radioactive fragments detected by fluorography (C).

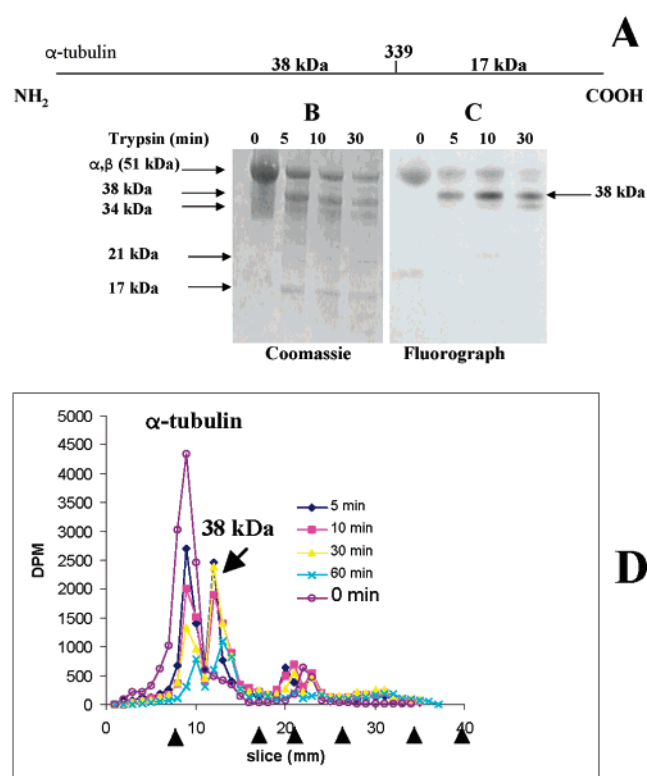


FIGURE 7: Limited digestion of probe 1-photolabeled tubulin with trypsin yields two labeled peptides. (A) Diagram demonstrating known cleavage sites within  $\alpha$ -tubulin when native tubulin is digested with trypsin. Tubulin (7.5  $\mu$ M) was incubated with 0.25  $\mu$ M (0.36  $\mu$ Ci) [<sup>3</sup>H]probe 1 for 30 min at RT and irradiated at 4 °C. After 2 h, the samples were digested with 0.8  $\mu$ g of trypsin at 30 °C for 0–60 min. After the reaction was stopped with 0.01 mM leupeptin, samples were resolved on 10–20% Tris-Tricine gels (B). Radioactive species within the gel was detected by fluorography (C) or by counting radioactivity within 1 mm gel slices (D). Arrowheads in panel D along the *x*-axis correspond to the position of the following molecular mass markers: 46, 29, 20, 14.5, 5.8, and 3.0 kDa (from left to right).

kDa corresponded to a fragment consistent with  $\alpha$ -tubulin digestion, a second at  $\sim$ 30 kDa originated from  $\beta$ -tubulin digestion, and a strongly stained Coomassie band at  $\sim$ 16 kDa corresponded to two 16 kDa fragments that originated from  $\alpha$ - and  $\beta$ -tubulin digestion. The radiolabel derived from probe 1 was found primarily in the 16 kDa peptide fragment (Figure 6 C). This result is in contrast to a previously described paclitaxel analogue or dolastatin 10 that labeled the 31 kDa or 3.5 kDa peptide fragment, respectively, derived from  $\beta$ -tubulin (9, 49). MS methods confirmed that the labeled 16 kDa formic acid fragment was from  $\alpha$ -tubulin. In preliminary studies, we have also digested tubulin after labeling it with probe 2. In this case, probe 2 did not bind to the 16 kDa fragment but to the 34.5 kDa fragment. Further mapping studies on probe 2 will be the subject of a later report.

Native tubulin was also digested with trypsin and subtilisin. Under these conditions, it is known that trypsin preferentially cleaves  $\alpha$ -tubulin after amino acid residue 339, producing two fragments that migrate at  $\sim$ 38 and 17 kDa (Figure 7A) (42, 50, 51). The latter fragment has a predicted molecular mass of 14 kDa, but migrates aberrantly in gels (34). The origin of the 34 and 21 kDa fragments is uncertain, but they are probably derived from  $\beta$ -tubulin (42). In our experiments,

photolabeled tubulin was digested for 5, 10, and 30 min with trypsin, and the resultant fragments were resolved in gels under conditions that allow  $\alpha$ - and  $\beta$ -tubulin to comigrate. On the basis of Coomassie staining of the gel, all the expected molecular mass species were observed (Figure 7B). In contrast, the major radiolabeled species were detected at  $\sim$ 51 and  $\sim$ 38 kDa and comigrated with the Coomassie-stained species (Figure 7C). There was a precursor–product relationship between the undigested tubulin (51 kDa) and the 38 kDa species, such that the ratio between the 51 and 38 kDa species decreased as the incubation time with trypsin increased (Figure 7C,D). The origin of a 19 kDa radiolabeled species, which was detected faintly in the autoradiogram of the gel (Figure 7C) and clearly in slices of the gel (Figure 7D), is unknown. However, it was present in the undigested sample and did not increase in intensity as the time of trypsin digestion was increased from 5 to 30 min. This may be an inherent fragment in the tubulin preparation. A minor radiolabeled species that migrated at approximately 34 kDa was observed after digestion for 10 and 30 min with trypsin. It is unlikely that this corresponds to the 34 kDa fragment derived from  $\beta$ -tubulin, since the 34 kDa Coomassie-stained band appeared within 5 min of trypsin digest, but it was not radiolabeled. Rather, it is more likely that the 34 kDa radiolabeled fragment is a partial digest of the 38 kDa fragment derived from  $\alpha$ -tubulin. Consistent with this, the intensity of the 34 kDa radiolabeled band increased as the 38 kDa band intensity decreased. However, we cannot rule out the possibility that the 34 kDa fragment derived from  $\beta$ -tubulin was labeled only after  $\beta$ -tubulin is cleaved by trypsin. Taken together with the formic acid digestion results, these data suggest that probe 1 labels between residues 307 and 339 of intact  $\alpha$ -tubulin.

To further resolve the probe 1 photoaffinity labeling domain, digestion of labeled tubulin was carried out with CNBr. CNBr cleaves peptide bonds on the carboxy-terminal side of methionine residues and, in these studies, was used to hydrolyze peptide bonds in polyacrylamide gels (52). On the basis of the sequence of  $\alpha$ -tubulin across a variety of species, it was predicted that  $\alpha$ -tubulin would be digested into 11 fragments by CNBr (Figure 8C). One of these fragments, which is conserved across rat, murine, and porcine  $\alpha$ -tubulin, had a predicted molecular mass of 7 kDa that spanned residues 314–376. To determine if the labeling site resided in the 7 kDa CNBr fragment,  $\alpha$ - and  $\beta$ -tubulin were separated in gels prior to digestion with CNBr (Figure 8A,B). Digestion of  $\alpha$ - and  $\beta$ -tubulin occurred, since many silver-stained fragments were observed (Figure 8B). Upon fluorography of the gel, one major and one minor radiolabeled species were observed at 7 and 8 kDa, respectively (Figure 8A). The identification of the 7 kDa species was confirmed using LysC digestion. Four main LysC peptide fragments were obtained and sequenced by mass spectrophotometric analysis. Figure 8 represents two of these fragments: a peptide containing amino acid residues 327–336 (Figure 8A) and a peptide containing amino acid residues 353–370 (Figure 9B). Unfortunately, the loss of tritium during this procedure, combined with the paucity of the label, did not allow us to resolve the binding site any further. Similar problems have been encountered in other photoaffinity studies (49, 53). The origin of the 8 kDa species is unknown, but likely to be a partial digest composed of the 1291 and



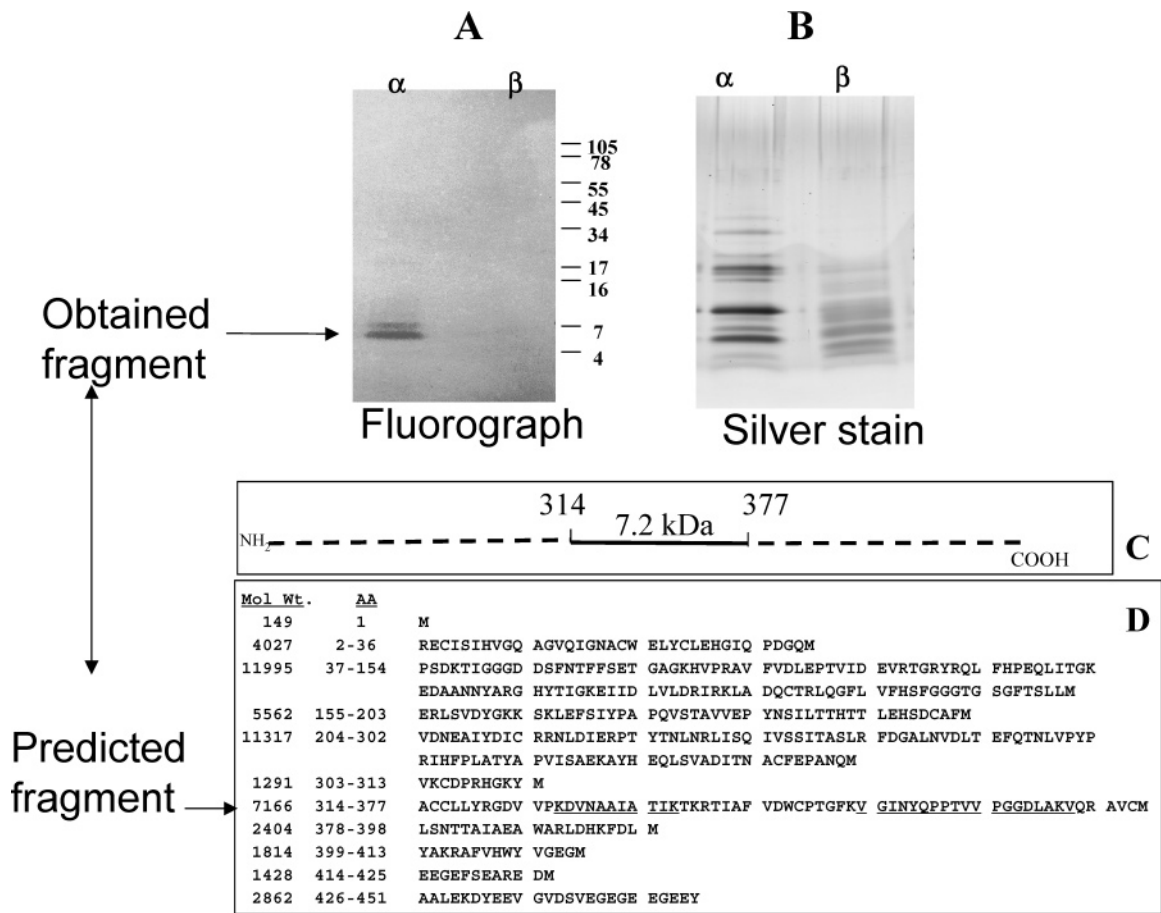


FIGURE 8: CNBr digestion of probe 1-photolabeled  $\alpha$ -tubulin. (A and B) After native tubulin was photolabeled as described above,  $\alpha$ - and  $\beta$ -tubulin were visualized in gels by Coomassie Blue staining. Protein within each species was extracted, reduced and alkylated, and then digested with 150 mg/mL CNBr in 70% formic acid at 37 °C as described in Materials and Methods. After 48 h, samples were resolved by SDS-PAGE fragments, and radiolabeled fragments were detected by fluorography (A) or proteins by silver staining (B): lanes 1 and 2, digestion of  $\alpha$ - and  $\beta$ -tubulin, respectively. (C) Diagram representing the predicted position of a 7 kDa labeled peptide fragment obtained after CNBr digestion. (D) Diagram showing all predicted CNBr fragments of rat  $\alpha$ -tubulin. The underlined areas are sequences that were confirmed using MS (Figure 8).

7166 Da CNBr fragments (Figure 8D). When the results of the digestion with formic acid, trypsin, and cyanogen bromide are considered, it is deduced that probe 1 labels  $\alpha$ -tubulin within residues 314–339.

DISCUSSION

Dolastatin 10, hemiasterlins, and cryptophycin A are naturally occurring small peptides that bind to tubulin, inhibit microtubule assembly, and are potent inhibitors of tumor cell growth (7). As shown here, tubulin appears to be the only intracellular target of hemiasterlin, since probe 1 bound exclusively and specifically to a protein that comigrated with tubulin when the reagent was incubated with cytosolic proteins derived from whole cells. Consistent with this, the same results were obtained if experiments were repeated using intact whole cells (data not shown). We further provide data to suggest that a portion of hemiasterlin interacts with  $\alpha$ -tubulin and places the binding site near the interdimer interface.

*Limitations of Photoaffinity Labeling with Hemiasterlin Analogues.* Before the implications of the work can be discussed, limitations of the methods need to be understood. The most outstanding issue is related to the photoaffinity probe itself. First, the benzophenone-containing photoprobe is an analogue of hemiasterlin and therefore may not mimic

the binding of hemiasterlin. Second, photoprobes when activated by irradiation experience mobility, and therefore, cross-linking can occur in a region(s) that is not the true binding site. Third, irradiation, which is required to photo-activate the probe, may alter tubulin itself and may account for nonspecific binding which has been observed for a photoactive vinblastine probe containing an azido group (54). The latter is of little concern, since irradiation of benzophenone derivatives at 350 nm nearly eliminates the potential for photodestruction of proteins, which may occur at shorter wavelengths used for azido-containing probes (55).

We do not believe the first objection is of major concern. Total synthesis of hemiasterlin has allowed the evaluation of the activity of a variety of hemiasterlin analogues. It is known that the so-called A amino acid of hemiasterlin, which contains an *N*-methylindole that is replaced with the benzophenone probe found in probe 1, can also be substituted with a phenyl group and retain potent antimicrotubule activity (17, 18). This led to the identification of SPA-110, also known as HTI-286 (18, 21), which is a potent antimicrotubule agent that is being developed clinically for use in cancer patients. In addition, extensive SAR studies in this region showed that potent activity can be retained if the phenyl group is replaced with many other substituents, including large groups such as biphenyl contained in probe 1, but is

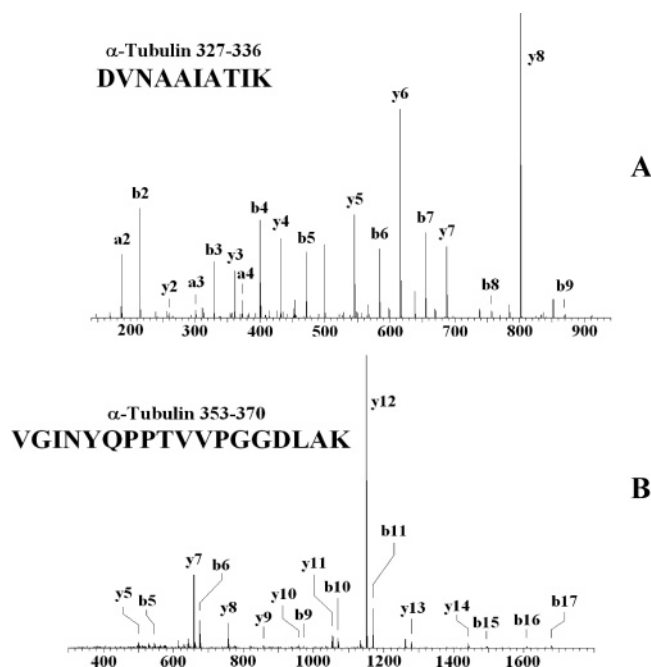


FIGURE 9: MS analysis of CNBr fragments derived from  $\alpha$ -tubulin. The 7 kDa CNBr gel fragment was further digested with LysC as described in Materials and Methods. Peptides were separated on HPLC using a 4 to 60% solvent B (0.1 M acetic acid, 90% ACN, and  $H_2O$ ; solvent A, 0.1 M acetic acid and  $H_2O$ ) gradient. The mass spectrometer was operated to acquire both MS and MS/MS spectra. Peptide sequences were determined by matching the fragment ion spectra against the nonredundant NCBI protein database using the Sequest search algorithm provided by Thermo-Finnigan.

substantially reduced if replaced by a methyl or hydroxyl group (18). Since the reactive group within the benzophenone is the ketone (55–57), this places the reactive group close to the phenyl ring within HTI-286. Beyond this, HTI-286 and the photoprobes used here have high affinity for tubulin, block polymerization of purified brain tubulin, and are potent inhibitors of cell growth. Probe 1 may provide more reliable data, since its affinity for tubulin and its antiproliferative potency in cells are more similar to those of HTI-286 than to those of probe 2. In addition, the interpretation of the data for probe 2 may be complicated since the benzophenone is added to the *tert*-butyl group in the B-region of hemiasterlin.

The second objection is more problematic, since it is possible that photoaffinity probes, when activated, can cross-link to reactive groups outside the binding domain (55). However, in contrast to other photoreactive groups such as azides, irradiation of benzophenone leads to a reactive excited state that reverts back to the ground state in the absence of an abstractable proton. This feature, combined with the short lifetime of the excited state, precludes false labeling that might result from diffusion, especially for high-affinity binders such as these photoprobes (56, 57). Consistent with this approach, photoaffinity analogues of paclitaxel have been useful in mapping binding domains of  $\beta$ -tubulin (49, 58) that have been substantiated by crystallographic analysis of zinc-induced assembled tubulin (3.5 Å) in the presence of paclitaxel (5). In addition, photoaffinity analogues of colchicine have placed the putative binding site within  $\alpha$ -tubulin (59),  $\beta$ -tubulin (60, 61), or both subunits (62, 63), while the crystallographic data (4) and other biochemical data (64, 65) place the molecule at the intradimer interface.

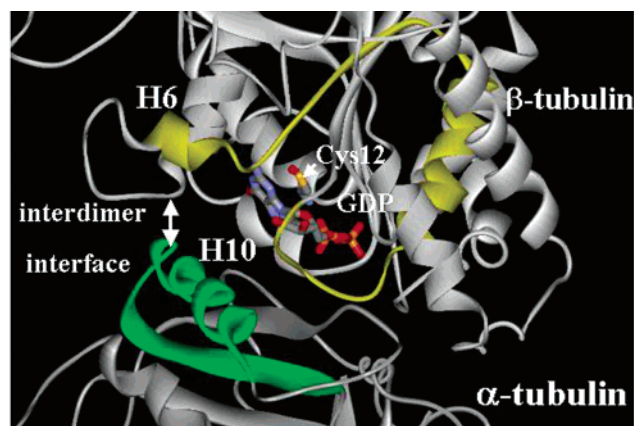


FIGURE 10: Location of the photoaffinity labeling region by probe 1 within the  $\alpha$ -tubulin– $\beta$ -tubulin interdimer interface (PDB entry 1JFF). The region of  $\alpha$ -tubulin that has been found to cross-link to probe 1 is colored green. The proposed photolabeling site for vinblastine is colored yellow, based on the work of Rai and Wolff (8). The position of the side chain of Cys<sup>12</sup> and GDP are shown in ball-and-stick format. H6 and H10 correspond to helices H6 and H10 of  $\beta$ - and  $\alpha$ -tubulin, respectively.

**Putative Hemiasterlin Binding Site.** Although the binding site for antimetabolic peptides and depsipeptides within tubulin is largely unknown, available evidence suggests it is distinct from the colchicine, taxane, and vinca alkaloid binding sites within tubulin. In particular, it has been established that dolastatin 10 (16), hemiasterlin (14), and cryptophycin 1 (15) noncompetitively inhibit the binding of radiolabeled vinblastine to tubulin. Furthermore, hemiasterlin competitively inhibited the binding of dolastatin 10 to tubulin (14). Like vinblastine, both dolastatin 10 and hemiasterlin inhibited nucleotide exchange (14, 16). Consistent with these data, cells selected for resistance to HTI-286 are cross-resistant to dolastatin 10 and vinca alkaloids, but have little resistance (or supersensitivity) to taxanes and colchicine (19, 20). Bai et al. hypothesized that the peptide binding site is distinct from, but in the proximity of, the vinca site and the exchangeable nucleotide site within  $\beta$ -tubulin (16). In support of this hypothesis, (a) vinca alkaloid photoaffinity probes bind  $\alpha$ - and  $\beta$ -tubulin (54, 66) or more specifically only  $\beta$ -tubulin, when using probes that require irradiation by wavelengths that would not perturb tubulin (8), (b) Cys<sup>12</sup> of  $\beta$ -tubulin is the major cross-linking site of exchangeable GTP (67, 68), (c) dolastatin 10 photoaffinity labels the 31 N-terminal amino acids of  $\beta$ -tubulin (9), and (d) a photoreactive probe for rhizoxin, which competitively inhibits binding of vinblastine to tubulin, labels  $\beta$ -tubulin (69).

The data presented here suggest that the hypothesis must be modified since a photoaffinity analogue of hemiasterlin cross-links exclusively within  $\alpha$ -tubulin. Consistent with the previous data, photoaffinity labeling is competed by vinblastine and dolastatin 10, but not other antimicrotubule agents such as paclitaxel or colchicine that bind to  $\beta$ -tubulin in a distinct location compared with vinca alkaloids. A major hemiasterlin photoaffinity binding site is located within residues 314–339 of  $\alpha$ -tubulin that, based on the electron micrographic crystal structure (3.5 Å) of zinc-induced tubulin sheets (5, 25), corresponds to S8 (residues 311–321) to H10 (residues 324–336) (Figure 10, region highlighted in green). The region is almost perfectly conserved within porcine, rat, and murine species (46), while it is approximately 80%

divergent from the corresponding region in  $\beta$ -tubulin within these species and may help explain why  $\beta$ -tubulin is not labeled with probe 1 or 2. The location of the cross-linking site for probe 2 is distinct compared with probe 1 and is the subject of a future report.

The H10 domain of  $\alpha$ -tubulin is involved in establishing both longitudinal and lateral protofilament contacts of tubulin subunits (25). The longitudinal interaction is particularly interesting since helix H10 of  $\alpha$ -tubulin interacts across the interdimer interface with helix H6 (Figure 10) and the H6–H7 loop of  $\beta$ -tubulin. Helix 6 and the H6–H7 loop of  $\beta$ -tubulin correspond to residues 204–213 and 214–221, respectively (5), and therefore, helix H6 is contained within a vinblastine photoaffinity labeling site restricted to residues 175–213 of  $\beta$ -tubulin (Figure 10, region highlighted in yellow) as well as the putative binding pocket for cryptophycin 52 (23). On the basis of molecular dynamics simulations and docking studies, the same region within  $\beta$ -tubulin has been implicated as a common binding domain for several antimitotic peptides, including dolastatin 10 and hemiasterlin (24). The proximity of putative vinblastine and hemiasterlin contact sites would explain why hemiasterlin noncompetitively inhibits binding of vinblastine to tubulin (14). Beyond this, the proximity of the exchangeable GTP site may explain why hemiasterlin and vinblastine alter GTP hydrolysis. Further resolution of the exact binding site within the S8–H10 region is required to refine the model, but because of the paucity of labeling, we have not been able to resolve the site further.

Since the 31 N-terminal amino acids of  $\beta$ -tubulin cross-link with dolastatin 10, and ultraviolet irradiation specifically activates sulfhydryl residues within Cys<sup>12</sup> of  $\beta$ -tubulin (67), Bai et al. suggest that the sulfhydryl residue with the thiazole ring of dolastatin 10 and Cys<sup>12</sup> may form a disulfide bond (9). The location of the sulfur atom within Cys<sup>12</sup> is shown in yellow within Figure 10 (behind the GDP molecule). Consistent with this, (a) auristatin-PE, which is a highly related dolastatin 10 analogue but does not contain a thiazole ring, has little or no cross-linking ability, (b) prior cross-linking between tubulin and GTP, which is known to cross-link at Cys<sup>12</sup> (67, 68), inhibited cross-linking of dolastatin 10 to tubulin, and (c) DTT inhibited formation of the cross-link between dolastatin 10 and tubulin. On the basis of extensive structure–activity relationships established for HTI-286 (18), we have observed similarities in the structure of tripeptide HTI-286 with the first three amino acids of the pentapeptide, dolastatin 10. In fact, hybrids of HTI-286 and the amine portion of dolastatin 10 were potent antimicrotubule agents (70). These observations support a superimposition of dolastatin 10 onto a low-energy conformation of HTI-286 (Figure 11). As the thiazole ring of dolastatin 10 and the benzophenone group of photoprobe 1 are diametrically opposed, one can place the photoreactive benzophenone group in  $\alpha$ -tubulin while having the thiazole group of dolastatin 10 in contact with Cys<sup>12</sup> of  $\beta$ -tubulin. Therefore, we propose that hemiasterlin is likely to bind within  $\alpha$ -tubulin or may span the  $\alpha$ -tubulin– $\beta$ -tubulin interdimer interface. If the latter is true, then the hemiasterlin binding site may compose a tetramer (two tubulin dimers). It is in contrast to colchicine that binds at the  $\alpha$ -tubulin– $\beta$ -tubulin intradimer interface and need only bind to the tubulin dimer (4). Recent modeling studies with hemiasterlin and other peptides that

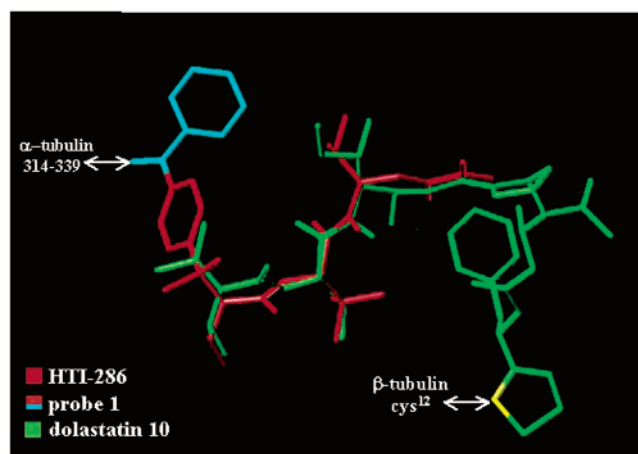


FIGURE 11: Overlay of HTI-286, photoprobe 1, and dolastatin 10. Superimposition of one of the minimum energy conformations of HTI-286 (red) with a low-energy conformation of dolastatin 10 (green). The sulfur atom within the thiazole of dolastatin is colored yellow. The additional portion of probe 1 added onto HTI-286 is colored blue. The proposed contact sites with tubulin are shown.

interact with tubulin support this proposal (24). They report that the binding site for hemiasterlin, dolastatin 10, cryptophycin, and phomopsin bind within only  $\beta$ -tubulin. However, the carbon within the R group of the first amino acid of hemiasterlin (within the phenyl ring), which would reside close to the aromatic group within the benzophenone probe, is only  $\sim 2.5$  Å from C<sub>ε</sub> of Lys<sup>326</sup> of  $\alpha$ -tubulin and within the predicted photoaffinity contact site. A more refined model of probe 1 or hemiasterlin docked into tubulin using these data, NMR, SAR, and modeling data will be in forthcoming reports.

If hemiasterlin were to bind at the interdimer interface, it would help explain why high concentrations of dolastatin 10 and hemiasterlin induce purified tubulin to form rings composed of 14  $\alpha$ – $\beta$  dimers (approximately 44 nm in diameter) (71) while cryptophycins induce rings composed of 8–9  $\alpha$ – $\beta$  dimers (approximately 20 nm in diameter) (23, 72). On the basis of the tubulin dimer crystal structure and the projected density map of the ring from cryoelectron microscopy, two points of curvature are found in cryptophycin-induced tubulin rings: at the intradimer interface and at the interdimer interface (72). We speculate that the degree of the interdimer bend would depend on which way each peptide is docked into the interdimer interface and may account for the diversity of ring size that has been observed.

**Comparison of Stathmin and Hemiasterlin Binding Sites in Tubulin.** The cross-linking domain for probe 1 within  $\alpha$ -tubulin shares striking similarity to that reported for the stathmin/OP18 protein. Stathmin/OP18 is a highly conserved 149-amino acid cytosolic phosphoprotein that directly interacts with tubulin, induces depolymerization of microtubules in vitro and in intact cells, and is overexpressed in leukemias, advanced breast cancer, and ovarian cancer (73). Eighty to ninety percent of stathmin can be cross-linked to  $\alpha$ -tubulin, and 10–20% is cross-linked to  $\beta$ -tubulin (74). Within  $\alpha$ -tubulin, the N-terminus of stathmin cross-links to residues 321–339 (26) or 303–335 (27) and contacts residues 333–355 of  $\alpha$ -tubulin using crystallographic methods (4). However, the rest of the molecule binds along the entire longitudinal length of the  $\alpha$ – $\beta$  dimer based on cocrystallization experiments (4, 75). Since stathmin and



HTI-286 induce depolymerization of tubulin and both molecules appear to bind to the H10 region of  $\alpha$ -tubulin, these data raise the possibility that the tripeptide HTI-286, and perhaps other lower-molecular mass peptides (i.e., dolastatin 10), mimic stathmin. Since stathmin either sequesters tubulin dimers or stimulates microtubule plus-end catastrophe (73), these findings suggest that HTI-286 may act in a fashion similar to that of stathmin.

**Effects of Temperature on Competition of Photoprobe Labeling.** On the basis of our competition experiments, it was found that taxanes and colchicine do not alter the binding of probe 1 at RT but can enhance the binding of probe 1 at 37 °C. The effect was not observed with other antimicrotubule agents. The basis for this effect is not understood. Higher temperatures enhance the binding of colchicine to tubulin. (76) Thus, high temperature and colchicine may further stabilize the tubulin dimer and enhance hemiasterlin binding. On the other hand, paclitaxel also enhances the polymerization of tubulin which suggests that hemiasterlin may bind microtubules. These findings suggest that it would be useful in further studies to determine the amount of hemiasterlin bound to tubulin dimers, or higher-order structures such as tetramers, rings, or microtubules.

**Interaction of the C-Terminus of Tubulin with the Hemiasterlin Binding Site.** The experiments with subtilisin are interesting since they suggest that there is an interaction of the C-terminus of  $\alpha$ -tubulin with the hemiasterlin photolabeling site. However, it is unlikely that the C-terminus of  $\alpha$ -tubulin contains a major labeling site, since the level of labeling was not markedly reduced if enzymatic removal of the C-terminus region was done before photolabeling tubulin with probe 1. Rather, if digestion was carried out after photolabeling (or after incubation with high concentrations of non-radiolabeled probe 1), subtilisin digestion of only  $\alpha$ -tubulin was inhibited. These data independently suggest that hemiasterlin interacts with  $\alpha$ -tubulin, although the exact mechanism of action remains to be determined.

In conclusion, the results presented here suggest that hemiasterlins have a binding site in  $\alpha$ -tubulin. Future studies using probes in different locations of HTI-286, along with molecular modeling and saturation transfer difference NMR, are likely to further elucidate the interaction of this antimicrotubule agent with tubulin. The hope is that this will lead to a better understanding of the mechanism of action of this and other peptidic molecules that interact with tubulin and ultimately help to design more clinically useful antimicrotubule agents to control cancer.

## ACKNOWLEDGMENT

We thank Drs. Malini Ravi and Yongbo Hu for help with molecular modeling. We also thank Drs. Susan Horwitz and George Orr for helpful discussion about this work. This work is dedicated to the memory of Dezider Grunberger.

## REFERENCES

- Rowinsky, E. K., and Tolcher, A. W. (2001) in *Cancer Principles and Practice* (Devita, V. T., Jr., Hellman, S., and Rosenberg, S. A., Eds.) pp 431–452, Lippincott Williams and Wilkins, Philadelphia.
- Downing, K. H. (2000) Structural basis for the interaction of tubulin with proteins and drugs that affect microtubule dynamics, *Annu. Rev. Cell Dev. Biol.* 16, 89–111.
- Jordan, M. A. (2002) Mechanism of action of antitumor drugs that interact with microtubules and tubulin, *Curr. Med. Chem.: Anti-Cancer Agents* 2, 1–17.
- Ravelli, R. B., Gigant, B., Curmi, P. A., Jourdain, I., Lachkar, S., Sobel, A., and Knossow, M. (2004) Insight into tubulin regulation from a complex with colchicine and a stathmin-like domain, *Nature* 428, 198–202.
- Lowe, J., Li, H., Downing, K. H., and Nogales, E. (2001) Refined structure of  $\alpha,\beta$ -tubulin at 3.5 Å resolution, *J. Mol. Biol.* 313, 1045–1057.
- Nettles, J. H., Li, H., Cornett, B., Krahn, J. M., Snyder, J. P., and Downing, K. H. (2004) The binding mode of epothilone A on  $\alpha,\beta$ -tubulin by electron crystallography, *Science* 305, 866–869.
- Hamel, E., and Covell, D. G. (2002) Antimitotic peptides and depsipeptides, *Curr. Med. Chem.: Anti-Cancer Agents* 2, 19–53.
- Rai, S. S., and Wolff, J. (1996) Localization of the vinblastine-binding site on  $\beta$ -tubulin, *J. Biol. Chem.* 271, 14707–14711.
- Bai, R., Covell, D. G., Taylor, G. F., Kepler, J. A., Copeland, T. D., Nguyen, N. Y., Pettit, G. R., and Hamel, E. (2004) Direct photoaffinity labeling by dolastatin 10 of the amino-terminal peptide of  $\beta$ -tubulin containing cysteine 12, *J. Biol. Chem.* 279, 30731–30740.
- Talpir, R., Benayahu, Y., Kashman, Y., Pannell, L., and Schleyer, M. (1994) Hemiasterlin and geodiamolide TA: Two new cytotoxic peptides from the marine sponge hemiasterella minor (Kirkpatrick), *Tetrahedron Lett.* 35, 4453–4456.
- Gamble, W. R., Durso, N. A., Fuller, R. W., Westergaard, C. K., Johnson, T. R., Sackett, D. L., Hamel, E., Cardellina, J. H., II, and Boyd, M. R. (1999) Cytotoxic and tubulin-interactive hemiasterlins from *Auleta* sp. and *Siphonochalina* spp. sponges, *Bioorg. Med. Chem.* 7, 1611–1615.
- Coleman, J. E., Dilip De Silva, E., Kong, F., Andersen, R. J., and Allen, T. M. (1995) Cytotoxic peptides from the marine sponge *Cymbastela* sp, *Tetrahedron* 51, 10653–10662.
- Anderson, H. J., Coleman, J. E., Andersen, R. J., and Roberge, M. (1997) Cytotoxic peptides hemiasterlin, hemiasterlin A and hemiasterlin B induce mitotic arrest and abnormal spindle formation, *Cancer Chemother. Pharmacol.* 39, 223–226.
- Bai, R., Durso, N. A., Sackett, D. L., and Hamel, E. (1999) Interactions of the sponge-derived antimitotic tripeptide hemiasterlin with tubulin: Comparison with dolastatin 10 and cryptophycin 1, *Biochemistry* 38, 14302–14310.
- Bai, R., Schwartz, R. E., Kepler, J. A., Pettit, G. R., and Hamel, E. (1996) Characterization of the interaction of cryptophycin 1 with tubulin: Binding in the Vinca domain, competitive inhibition of dolastatin 10 binding, and an unusual aggregation reaction, *Cancer Res.* 56, 4398–4406.
- Bai, R. L., Pettit, G. R., and Hamel, E. (1990) Binding of dolastatin 10 to tubulin at a distinct site for peptide antimitotic agents near the exchangeable nucleotide and vinca alkaloid sites, *J. Biol. Chem.* 265, 17141–17149.
- Nieman, J., Coleman, J., Wallace, D., Piers, E., Lim, L. Y., Roberge, M., and Andersen, R. J. (2003) Synthesis and antimitotic/cytotoxic activity of hemiasterlin analogs, *J. Nat. Prod.* 66, 183–199.
- Zask, A., Birnberg, G., Cheung, K., Kaplan, J., Niu, C., Norton, E., Suayan, R., Yamashita, A., Cole, D., Tang, Z., Krishnamurthy, G., Williamson, R., Khafizova, G., Musto, S., Hernandez, R., Annable, T., Yang, X., Discafani, C., Beyer, C., Greenberger, L. M., Loganzo, F., and Ayral-Kaloustian, S. (2004) Synthesis and biological activity of analogues of the antimicrotubule agent N $\beta$ , $\beta$ -trimethyl-L-phenylalanyl-N $^1$ -[(1S,2E)-3-carboxy-1-isopropylbut-2-enyl]-N $^1$ ,3-dimethyl-L-valinamide (HTI-286), *J. Med. Chem.* 47, 4774–4786.
- Loganzo, F., Hari, M., Annable, T., Tan, X., Morilla, D. B., Musto, S., Zask, A., Kaplan, J., Minnick, A. A., Jr., May, M. K., Ayral-Kaloustian, S., Poruchynsky, M. S., Fojo, T., and Greenberger, L. M. (2004) Cells resistant to HTI-286 do not overexpress P-glycoprotein but have reduced drug accumulation and a point mutation in  $\alpha$ -tubulin, *Mol. Cancer Ther.* 3, 1319–1327.
- Poruchynsky, M. S., Kim, J. H., Nogales, E., Annable, T., Loganzo, F., Greenberger, L. M., Sackett, D. L., and Fojo, T. (2004) Tumor cells resistant to a microtubule-depolymerizing hemiasterlin analogue, HTI-286, have mutations in  $\alpha$ - or  $\beta$ -tubulin and increased microtubule stability, *Biochemistry* 43, 13944–13954.
- Loganzo, F., Discafani, C. M., Annable, T., Beyer, C., Musto, S., Hari, M., Tan, X., Hardy, C., Hernandez, R., Baxter, M., Singanallure, T., Khafizova, G., Poruchynsky, M. S., Fojo, T.,

- Nieman, J. A., Ayral-Kaloustian, S., Zask, A., Andersen, R. J., and Greenberger, L. M. (2003) HTI-286, a synthetic analogue of the tripeptide hemiasterlin, is a potent antimicrotubule agent that circumvents P-glycoprotein-mediated resistance in vitro and in vivo, *Cancer Res.* 63, 1838–1845.
22. Ratain, M. J., Undevia, S., Janisch, L., Roman, S., Mayer, P., Buckwalter, M., Foss, D., Hamilton, B. L., Fischer, J., and Bukowski, R. M. (2003) Phase I and pharmacological study of HTI-286, a novel antimicrotubule agent: Correlation of neutropenia with time above threshold plasma concentration, *Proc. Am. Soc. Clin. Oncol.*, Abstract 516.
23. Barbier, P., Gregoire, C., Devred, F., Sarrazin, M., and Peyrot, V. (2001) In vitro effect of cryptophycin 52 on microtubule assembly and tubulin: Molecular modeling of the mechanism of action of a new antimitotic drug, *Biochemistry* 40, 13510–13519.
24. Mitra, A., and Sept, D. (2004) Localization of the antimitotic peptide and depsipeptide binding site on  $\beta$ -tubulin, *Biochemistry* 43, 13955–13962.
25. Nogales, E., Whittaker, M., Milligan, R. A., and Downing, K. H. (1999) High-resolution model of the microtubule, *Cell* 96, 79–88.
26. Muller, D. R., Schindler, P., Towbin, H., Wirth, U., Voshol, H., Hoving, S., and Steinmetz, M. O. (2001) Isotope-tagged cross-linking reagents. A new tool in mass spectrometric protein interaction analysis, *Anal. Chem.* 73, 1927–1934.
27. Wallon, G., Rappsilber, J., Mann, M., and Serrano, L. (2000) Model for stathmin/OP18 binding to tubulin, *EMBO J.* 19, 213–222.
28. Kaplan, J. A., Nunes, M., Ayral-Kaloustian, S., Krishnamurthy, G., Loganzo, F., Greenberger, L. M., Minnick, A., May, M., and Zask, A. (2002) Hemiasterlin photoaffinity ligands: [ $^3\text{H}$ ]Benzophenone analogs of HTI-286, *Natl. Med. Chem. Symp.*, Abstract 49.
29. Crabtree, R. H., Demou, P. C., Eden, D., Mihelcic, J. M., Parnell, C. A., Quirk, J. M., and Morris, G. E. (1982) Dihydrodiolefin and solvent complexes of iridium and the mechanisms of olefin hydrogenation and alkane dehydrogenation, *J. Am. Chem. Soc.* 104, 699–7001.
30. Crabtree, R. H. (1990) Dihydrogen complexes: Some structural and chemical studies, *Acc. Chem. Res.* 23, 95–101.
31. Heys, R. (1992) Investigation of  $[\text{IrH}_2(\text{Me}_2\text{CO})_2(\text{PPH}_3)_2]\text{BF}_4$  as a catalyst of hydrogen isotope exchange of substrates in solution, *J. Chem. Soc., Chem. Commun.*, 680–681.
32. Hesk, D., Das, P. R., and Evans, B. (1995) Deuteration of acetanilides and other substituted aromatics using  $[\text{Ir}(\text{COD})-(\text{Cy}3\text{P})(\text{Py})]\text{PF}_6$  as catalyst, *J. Labelled Compd. Radiopharm.* 36, 497–502.
33. Shu, A. Y. L., Chen, W., and Heys, J. R. (1996) Organoiridium catalyzed hydrogen isotope exchange: Ligand effects on catalyst activity and regioselectivity, *J. Organomet. Chem.* 524, 87–93.
34. Chen, W., Ganes, K. T., Levinson, S. H., Saunders, D., Senderoff, S. G., Shu, A. Y. L., Villani, A. J., and Heys, J. R. (1997) Direct tritium labeling of multifunctional compounds using organoiridium catalysis, *J. Labelled Compd. Radiopharm.* 39, 291–298.
35. Shu, A. Y. L., Saunders, D., Levinson, S. H., Landvatter, S. W., Mahoney, A., Senderoff, S. G., Mack, J. F., and Heys, J. R. (1999) Direct tritium labeling of multifunctional compounds using organoiridium catalysis. 2, *J. Labelled Compd. Radiopharm.* 42, 797–807.
36. Krishnamurthy, G., Cheng, W., Lo, M. C., Aulabaugh, A., Razinkov, V., Ding, W., Loganzo, F., Zask, A., and Ellestad, G. (2003) Biophysical characterization of the interactions of HTI-286 with tubulin heterodimer and microtubules, *Biochemistry* 42, 13484–13495.
37. Shevchenko, A., Wilm, M., Vorm, O., and Mann, M. (1996) Mass spectrometric sequencing of proteins silver-stained polyacrylamide gels, *Anal. Chem.* 68, 850–858.
38. Andersen, R. J., Coleman, J. E., Piers, E., and Wallace, D. J. (1997) Total synthesis of (–)-hemiasterlin, a structurally novel tripeptide that exhibits potent cytotoxic activity, *Tetrahedron Lett.* 38, 317–320.
39. Hamel, E. (1996) Antimitotic natural products and their interactions with tubulin, *Med. Res. Rev.* 16, 207–231.
40. Redeker, V., Melki, R., Prome, D., Le Caer, J. P., and Rossier, J. (1992) Structure of tubulin C-terminal domain obtained by subtilisin treatment. The major  $\alpha$  and  $\beta$  tubulin isotypes from pig brain are glutamylated, *FEBS Lett.* 313, 185–192.
41. Serrano, L., de la Torre, J., Maccioni, R. B., and Avila, J. (1984) Involvement of the carboxyl-terminal domain of tubulin in the regulation of its assembly, *Proc. Natl. Acad. Sci. U.S.A.* 81, 5989–5993.
42. Sackett, D. L., and Wolff, J. (1986) Proteolysis of tubulin and the substructure of the tubulin dimer, *J. Biol. Chem.* 261, 9070–9076.
43. Rai, S. S., and Wolff, J. (1998) The C terminus of  $\beta$ -tubulin regulates vinblastine-induced tubulin polymerization, *Proc. Natl. Acad. Sci. U.S.A.* 95, 4253–4257.
44. Johnson, K. A., and Borisy, G. G. (1979) Thermodynamic analysis of microtubule self-assembly in vitro, *J. Mol. Biol.* 133, 199–216.
45. Sonderegger, P., Jaussi, R., Gehring, H., Brunschweiler, K., and Christen, P. (1982) Peptide mapping of protein bands from polyacrylamide gel electrophoresis by chemical cleavage in gel pieces and re-electrophoresis, *Anal. Biochem.* 122, 298–301.
46. Stanchi, F., Corso, V., Scannapieco, P., Ievolella, C., Negrisolo, E., Tiso, N., Lanfranchi, G., and Valle, G. (2000) TUBA8: A new tissue-specific isoform of  $\alpha$ -tubulin that is highly conserved in human and mouse, *Biochem. Biophys. Res. Commun.* 270, 1111–1118.
47. Chau, M. F., Radeke, M. J., de Ines, C., Barasoain, I., Kohlstaedt, L. A., and Feinstein, S. C. (1998) The microtubule-associated protein  $\tau$  cross-links to two distinct sites on each  $\alpha$  and  $\beta$  tubulin monomer via separate domains, *Biochemistry* 37, 17692–17703.
48. Hall, J. L., Dudley, L., Dobner, P. R., Lewis, S. A., and Cowan, N. J. (1983) Identification of two human  $\beta$ -tubulin isotypes, *Mol. Cell. Biol.* 3, 854–862.
49. Rao, S., Orr, G. A., Chaudhary, A. G., Kingston, D. G., and Horwitz, S. B. (1995) Characterization of the taxol binding site on the microtubule. 2-(m-Azidobenzoyl)taxol photolabels a peptide (amino acids 217–231) of  $\beta$ -tubulin, *J. Biol. Chem.* 270, 20235–20238.
50. Serrano, L., Avila, J., and Maccioni, R. B. (1984) Limited proteolysis of tubulin and the localization of the binding site for colchicine, *J. Biol. Chem.* 259, 6607–6611.
51. Mandelkow, E. M., Herrmann, M., and Ruhl, U. (1985) Tubulin domains probed by limited proteolysis and subunit-specific antibodies, *J. Mol. Biol.* 185, 311–327.
52. Sokolov, B. P., Sher, B. M., and Kalinin, V. N. (1989) Modified method for peptide mapping of collagen chains using cyanogen bromide-cleavage of protein within polyacrylamide gels, *Anal. Biochem.* 176, 365–367.
53. Loeb, C., Combeau, C., Ehret-Sabatier, L., Breton-Gilet, A., Faucher, D., Rousseau, B., Commercon, A., and Goeldner, M. (1997) [ $^3\text{H}$ ](azidophenyl)ureido taxoid photolabels peptide amino acids 281–304 of  $\alpha$ -tubulin, *Biochemistry* 36, 3820–3825.
54. Safa, A. R., Hamel, E., and Felsted, R. L. (1987) Photoaffinity labeling of tubulin subunits with a photoactive analogue of vinblastine, *Biochemistry* 26, 97–102.
55. Williams, N., Ackerman, S. H., and Coleman, P. S. (1986) Benzophenone-ATP: A photoaffinity label for the active site of ATPases, *Methods Enzymol.* 126, 667–682.
56. Fleming, S. A. (1995) Chemical Reagents in Photoaffinity Labeling, *Tetrahedron* 51, 12479–12520.
57. Dorman, G., and Prestwich, G. D. (1994) Benzophenone photo-phores in biochemistry, *Biochemistry* 33, 5661–5673.
58. Rao, S., He, L., Chakravarty, S., Ojima, I., Orr, G. A., and Horwitz, S. B. (1999) Characterization of the colchicine binding site on the microtubule. Identification of Arg(282) in  $\beta$ -tubulin as the site of photoincorporation of a 7-benzophenone analogue of Taxol, *J. Biol. Chem.* 274, 37990–37994.
59. Williams, R. F., Mumford, C. L., Williams, G. A., Floyd, L. J., Aivaliotis, M. J., Martinez, R. A., Robinson, A. K., and Barnes, L. D. (1985) A photoaffinity derivative of colchicine: 6'-(4'-Azido-2'-nitrophenylamino)hexanoyldeacetylcolchicine. Photolabeling and location of the colchicine-binding site on the  $\alpha$ -subunit of tubulin, *J. Biol. Chem.* 260, 13794–13802.
60. Bai, R., Pei, X. F., Boye, O., Getahun, Z., Grover, S., Bekisz, J., Nguyen, N. Y., Brossi, A., and Hamel, E. (1996) Identification of cysteine 354 of  $\beta$ -tubulin as part of the binding site for the A ring of colchicine, *J. Biol. Chem.* 271, 12639–12645.
61. Bai, R., Covell, D. G., Pei, X. F., Ewell, J. B., Nguyen, N. Y., Brossi, A., and Hamel, E. (2000) Mapping the binding site of colchicins on  $\beta$ -tubulin. 2-Chloroacetyl-2-demethylthiocolchicine covalently reacts predominantly with cysteine 239 and secondarily with cysteine 354, *J. Biol. Chem.* 275, 40443–40452.
62. Floyd, L. J., Barnes, L. D., and Williams, R. F. (1989) Photoaffinity labeling of tubulin with (2-nitro-4-azidophenyl)deacetylcolchi-

- cine: Direct evidence for two colchicine binding sites, *Biochemistry* 28, 8515–8525.
63. Wolff, J., Knipling, L., Cahnmann, H. J., and Palumbo, G. (1991) Direct photoaffinity labeling of tubulin with colchicine, *Proc. Natl. Acad. Sci. U.S.A.* 88, 2820–2824.
64. Shearwin, K. E., and Timasheff, S. N. (1994) Effect of colchicine analogues on the dissociation of  $\alpha\beta$  tubulin into subunits: The locus of colchicine binding, *Biochemistry* 33, 894–901.
65. Chaudhuri, A. R., Seetharamalu, P., Schwarz, P. M., Hausheer, F. H., and Luduena, R. F. (2000) The interaction of the B-ring of colchicine with  $\alpha$ -tubulin: A novel footprinting approach, *J. Mol. Biol.* 303, 679–692.
66. Nasioulas, G., Grammbitter, K., Himes, R. H., and Ponstingl, H. (1990) Interaction of a new photosensitive derivative of vinblastine, NAPAVIN, with tubulin and microtubules in vitro, *Eur. J. Biochem.* 192, 69–74.
67. Shivanna, B. D., Mejillano, M. R., Williams, T. D., and Himes, R. H. (1993) Exchangeable GTP binding site of  $\beta$ -tubulin. Identification of cysteine 12 as the major site of cross-linking by direct photoaffinity labeling, *J. Biol. Chem.* 268, 127–132.
68. Bai, R., Ewell, J. B., Nguyen, N. Y., and Hamel, E. (1999) Direct photoaffinity labeling of cysteine 211 or a nearby amino acid residue of  $\beta$ -tubulin by guanosine 5'-diphosphate bound in the exchangeable site, *J. Biol. Chem.* 274, 12710–12714.
69. Sawada, T., Kobayashi, H., Hashimoto, Y., and Iwasaki, S. (1993) Identification of the fragment photoaffinity-labeled with azidodansyl-rhizoxin as Met-363-Lys-379 on  $\beta$ -tubulin, *Biochem. Pharmacol.* 45, 1387–1394.
70. Zask, A., Kaplan, J., Beyer, C., Discafani, C., Musto, S., and Loganzo, F. (2003) Hybrids of the hemiasterlin analog HTI-286 and dolastatin are potent antimicrotubule agents, *Clin. Cancer Res.* 9, 6131s.
71. Boukari, H., Nossal, R., and Sackett, D. L. (2003) Stability of drug-induced tubulin rings by fluorescence correlation spectroscopy, *Biochemistry* 42, 1292–1300.
72. Watts, N. R., Cheng, N., West, W., Steven, A. C., and Sackett, D. L. (2002) The cryptophycin-tubulin ring structure indicates two points of curvature in the tubulin dimer, *Biochemistry* 41, 12662–12669.
73. Cassimeris, L. (2002) The oncoprotein 18/stathmin family of microtubule destabilizers, *Curr. Opin. Cell Biol.* 14, 18–24.
74. Larsson, N., Marklund, U., Gradin, H. M., Brattsand, G., and Gullberg, M. (1997) Control of microtubule dynamics by oncoprotein 18: Dissection of the regulatory role of multisite phosphorylation during mitosis, *Mol. Cell. Biol.* 17, 5530–5539.
75. Gigant, B., Curmi, P. A., Martin-Barbey, C., Charbaut, E., Lachkar, S., Lebeau, L., Siavoshian, S., Sobel, A., and Knossow, M. (2000) The 4 Å X-ray structure of a tubulin:stathmin-like domain complex, *Cell* 102, 809–816.
76. Luduena, R. F., Prasad, V., Roach, M. C., and Lacey, E. (1989) The interaction of phomopsin A with bovine brain tubulin, *Arch. Biochem. Biophys.* 272, 32–38.
77. Rai, S. S., and Wolff, J. (1997) Vinblastine-induced formation of tubulin polymers is electrostatically regulated and nucleated, *Eur. J. Biochem.* 250, 425–431.
78. Al-Bassam, J., Ozer, R. S., Safer, D., Halpain, S., and Milligan, R. A. (2002) MAP2 and  $\tau$  bind longitudinally along the outer ridges of microtubule protofilaments, *J. Cell Biol.* 157, 1187–1196.

BI0474766